

# Simultaneous Consensus Maximization and Model Fitting

Fei Wen, Hewen Wei, Yipeng Liu, and Peilin Liu

**Abstract**—Maximum consensus (MC) robust fitting is a fundamental problem in low-level vision to process raw-data. Typically, it firstly finds a consensus set of inliers and then fits a model on the consensus set. This work proposes a new formulation to achieve simultaneous maximum consensus and model estimation (MCME), which has two significant features compared with traditional MC robust fitting. First, it takes fitting residual into account in finding inliers, hence its lowest achievable residual in model fitting is lower than that of MC robust fitting. Second, it has an unconstrained formulation involving binary variables, which facilitates the use of the effective semidefinite relaxation (SDR) method to handle the underlying challenging combinatorial optimization problem. Though still nonconvex after SDR, it becomes biconvex in some applications, for which we use an alternating minimization algorithm to solve. Further, the sparsity of the problem is exploited in combination with low-rank factorization to develop an efficient algorithm. Experiments show that MCME significantly outperforms RANSAC and deterministic approximate MC methods at high outlier ratios. Besides, in rotation and Euclidean registration, it also compares favorably with state-of-the-art registration methods, especially in high noise and outliers. Code is available at <https://github.com/FWen/mcme.git>.

**Index Terms**—Maximum consensus, robust fitting, homography estimation, rotation registration, point-cloud registration, outlier removal.

## I. INTRODUCTION

**R**OBUST fitting is a fundamental problem in low-level vision to process raw data in the presence of outliers, which plays a critical role in modern vision geometry [1]–[4]. For robust fitting, the maximum consensus (MC) criterion is of the most popular and widely used. Given a set of raw measurements, MC aims to find a model that has the largest consensus on the measurements. Due to its importance, a number of methods have been proposed, including randomized methods, global methods and deterministic approximate methods.

Randomized methods, such as the classic RANSAC method [5] and its variants [6]–[10], typically use a hypothesize-and-verify procedure to fit the model on randomly sampled subsets and verify the model based on the size of measurements consistent with the model. A significant feature of randomized methods is that their solution quality is guaranteed in

probability depending on iteration number. In practical applications with affordable finite iterations, the solution quality is unpredictable and can be random in different runs due to their randomized nature. Global methods aim to find an optimum solution by global optimization algorithms. As the MC problem is intrinsically a combinatorial optimization problem, global optimum can only be guaranteed by searching based algorithms, such as branch-and-bound (BnB) search [11]–[13], tree search [14], and enumeration [15], [16]. Though optimum solution can be achieved, global methods do not scale to moderate to high dimensional problems. Deterministic approximate methods solve the MC problem approximately and deterministically, such as the convex relaxed method [17], reweighted method [18],  $\ell_0$  method [19], and exact penalty (EP) method [20, 21]. Moreover, deterministic outlier removal methods using  $\ell_\infty$  norm have been proposed in [22, 23]. These methods are computationally much more efficient than global methods, and meanwhile, some of them can achieve better solution quality than randomized methods [21].

Typically, MC robust fitting has two steps, firstly finding a consensus set of inliers and then fitting a model on the consensus set. Though has been shown to be effective in many applications, this two-step procedure does not take the distribution of fitting residual into account in finding the inlier set. To overcome this limitation, this work proposes a new single-step formulation for robust fitting to achieve simultaneous maximum consensus and model estimation (MCME).

Compared with traditional MC robust fitting, the new formulation brings two benefits. Firstly, it takes the fitting residual into account in identifying the inlier set for model fitting. As a result, we show that the lowest achievable fitting residual of MCME is lower than that of MC robust fitting. Secondly, the unconstrained formulation of MCME enables us to employ the effective semidefinite relaxation (SDR) approach to handle the underlying intractable combinatorial optimization problem. SDR is tighter than linear relaxation and it has been shown very effective in handling combinatorial problems [24, 25]. Though both formulations of MC and MCME are intrinsically binary combinatorial optimization problems (which are NP-hard), the unconstrained form of MCME facilitates the use of SDR to effectively solve the involved binary optimization problem.

The main contributions of this work are as follows. First, we propose the new formulation MCME. Second, we theoretically show that the lowest achievable fitting residual of MCME is lower than that of MC robust fitting. Third, a SDR embedding based algorithm is developed for MCME, in which the sparsity of the problem is exploited in combination with low-rank

F. Wen and P. Liu are with the Department of Electronic Engineering, Shanghai Jiao Tong University, Shanghai, China, 200240. E-mail: wenfei@sjtu.edu.cn; liupeilin@sjtu.edu.cn.

H. Wei is with Shanghai branch of the Southwest Institute of Electronics and Telecommunication Technology of China, Shanghai, China, 200434. Email: weihewen@tsinghua.org.cn. Y. Liu is with the School of Electronic Engineering, University of Electronic Science and Technology of China, Chengdu, China, 611731. E-mail: yipengliu@uestc.edu.cn.

Manuscript received xx, xx, 2020.

factorization to achieve high efficiency. Finally, experimental results on 2D and 3D registration are provided to demonstrate the favorable performance of MCME in comparison with previous state-of-the-art.

Note that there also exist a number of direct robust fitting methods, such as the M-estimators [26]–[28] and the robust registration methods [29]–[30]. These methods commonly use robust loss functions to mitigate the effect of outliers, but do not apply to the maximum consensus problem, i.e. do not identify inliers/outliers. As will be shown in Section 5.5 and 5.6, the proposed method outperforms such direct fitting methods. Moreover, the QUASAR method [31] for rotation search can be viewed as a special instance of MCME, which inspired us much. QUASAR is highly robust and performs well even in the presence of extreme outliers. But the adopted binary cloning strategy in its QCQP reformulation only applies to the rotation search problem. As will be detailed in Section 4.3, for the rotation search problem, our relaxed MCME formulation is tighter than that of QUASAR, while our algorithm is much more efficient (e.g., three orders of magnitude faster).

*Notations:*  $\mathbb{I}(\cdot) \in \{0, 1\}$  is the indicator function.  $\otimes$  and  $\circ$  stand for the Kronecker product and quaternion product, respectively.  $\mathbf{1}_N$  is an  $N$  dimension vector with all elements being unit, and  $\mathbf{0}$  is a zero vector or matrix with a proper size.  $\|\cdot\|$  and  $\|\cdot\|_p$  denotes the Euclidean and  $\ell_p$  norm, respectively.  $(\cdot)^T$  denotes transpose.  $\mathbb{S}^N$  is the set of  $N \times N$  real-valued symmetric matrices. For  $\mathbf{X} \in \mathbb{S}^N$ ,  $\mathbf{X} \succeq \mathbf{0}$  means that  $\mathbf{X}$  is semidefinite. Both  $\mathbf{X}(i, j)$  and  $X_{i, j}$  denote the  $(i, j)$ -th element of the matrix  $\mathbf{X}$ .  $\text{vec}(\cdot)$  is the vectorization operation of a matrix.

## II. PROPOSED FORMULATION

### A. From MC to MCME

Generally, MC robust fitting consists of two steps, firstly finding the largest consensus set, and then conducting model fitting on the obtained consensus set (inliers). Given a set of  $N$  measurements, MC aims to find a feasible model parameterized by  $\boldsymbol{\theta} \in \mathbb{R}^d$ , that is consistent with as many of the measurements as possible up to an inlier residual threshold  $\tau > 0$ , i.e., has the largest consensus set  $I$  as [1]

$$\text{MC : } \begin{aligned} & \max_{\boldsymbol{\theta} \in \mathbb{R}^d, I \subseteq \Omega} |I| \\ & \text{subject to } r_i(\boldsymbol{\theta}) \leq \tau, \quad \forall i \in I, \end{aligned} \quad (1)$$

where  $r_i(\boldsymbol{\theta})$  gives the residual of the  $i$ -th measurement with respect to the model parameter  $\boldsymbol{\theta}$ ,  $\Omega = \{1, 2, \dots, N\}$  is the index set of the measurements. Let  $I^*$  be a solution of (1), then  $I^*$  stands for the index set of the true inliers, while the complementary set of  $I^*$ , denoted by  $\Omega \setminus I^*$ , stands for the index set of the true outliers. Using some auxiliary binary variables  $\mathbf{s} = [s_1, \dots, s_N]^T \in \{0, 1\}^N$ , (1) can be reformulated into

$$\min_{\boldsymbol{\theta} \in \mathbb{R}^d, \mathbf{s} \in \{0, 1\}^N} \sum_{i=1}^N s_i \quad (2)$$

subject to  $r_i(\boldsymbol{\theta}) \leq \tau + s_i L$ ,  $\forall i \in \Omega$ ,

where  $L$  is a sufficient large positive constant.

For a solution of MC,  $s_i = 1$  means the  $i$ -th measurement is an outlier that should not be taken into account in model estimation, while  $s_i = 0$  means an inlier that should be used in model estimation. A solution  $\boldsymbol{\theta}$  of MC is a feasible solution of the model satisfying the inlier residual constraint, and hence a second step is commonly used to conduct model fitting on the identified consensus set (inliers).

Though has been widely shown to be effective, this two-step procedure does not take the distribution of inlier residual into account in finding the inlier set. To address this limitation, this work extends the MC formulation (2) to propose a new formulation to achieve simultaneously consensus maximization and model fitting in a single step. It simultaneously minimizes the number of outliers and the residual of model fitting as

$$\text{MCME : } \min_{\boldsymbol{\theta} \in \mathbb{R}^d, \mathbf{s} \in \{0, 1\}^N} \sum_{i=1}^N (1 - s_i) \Phi(r_i(\boldsymbol{\theta})) + \beta s_i, \quad (3)$$

where  $\Phi$  is a loss function of residual for model fitting,  $\beta > 0$  is a balance parameter that controls the tradeoff between the number of outliers and the fitting residual. Meanwhile, we also consider a generalized formulation of MCME as

$$\min_{\boldsymbol{\theta} \in \mathbb{R}^d, \mathbf{s} \in \{0, 1\}^N} \Psi(\boldsymbol{\theta}, \mathbf{s}) + \beta \mathbf{1}_N^T \mathbf{s}, \quad (4)$$

where  $\Psi$  is a generalized model fitting cost depending on  $\mathbf{s}$  and  $\boldsymbol{\theta}$ , which includes the fitting cost in (3) as a special case. This generalization makes the MCME formulation adapt to diverse applications, which will be detailed in Section 4.

This MCME formulation can be viewed as a natural extension of the MC formulation (2), and both are embedded with a binary optimization problem. A significant feature of MCME is that the residual constraint in MC is removed, which leads to an unconstrained formulation. Clearly, in MCME only the inliers (identified by  $s_i = 0$ ) are taken into account in fitting the model. Unlike the  $\boldsymbol{\theta}$  solution of MC being a feasible solution of the model under inlier residual constraint, the  $\boldsymbol{\theta}$  solution of MCME is the desired model fitting result on the identified inliers.

MCME uses a parameter  $\beta$  to balance the number of inliers/outliers against the model fitting residual, by which the residual constraint in MC is removed to get an unconstrained formulation. Obviously, a larger value of  $\beta$  would result in a larger number of  $s_i$ 's being zero, i.e., more identified inliers (which are not necessary to be true inliers). That is a too large value of  $\beta$  would yield a larger consensus size than  $|I^*|$  and include some true outliers, while a too small value of  $\beta$  would yield a smaller consensus size than  $|I^*|$  and exclude some true inliers. Hence, the selection of  $\beta$  is crucial for MCME to perform satisfactorily.

The following two results explicitly indicate how to select  $\beta$  based on the distribution of inliers.

*Proposition 1.* The MCME problem (3) is equivalent to

$$\min_{\boldsymbol{\theta} \in \mathbb{R}^d} \sum_{i=1}^N \bar{\Phi}_\beta(r_i(\boldsymbol{\theta})), \quad (5)$$

where  $\bar{\Phi}_\beta$  is a truncated version of  $\Phi$  at the threshold of  $\beta$  as

$$\bar{\Phi}_\beta(\cdot) = \min(\Phi(\cdot), \beta).$$

*Remark 1.* This result follows straightforwardly from the fact that,  $\min_{s_i \in \{0,1\}} (1 - s_i)\Phi(\cdot) + \beta s_i$  is equivalent to  $\min(\Phi(\cdot), \beta)$ . It indicates that the MCME formulation is in fact equivalent to minimizing the summation of truncated residuals, by using a truncated loss function. It computes a solution only using the measurements with small residuals (i.e., less than  $\beta$ ), while discarding the measurements with residuals larger than  $\beta$ . From this point of view,  $\beta$  can be easily selected as a threshold which tightly upper bounds the fitting residual of the true inliers. For example, if there exists a proper bound  $\tau$  such that  $r_i(\boldsymbol{\theta}) \leq \tau$  for  $\forall i \in I^*$  with a high probability for the true parameter  $\boldsymbol{\theta}$ , it is reasonable to choose  $\beta = \Phi(\tau)$ .

The following result further shows MCME can be viewed as an approximate maximum likelihood (ML) estimator under certain distribution assumption of inliers and outliers.

*Proposition 2.* Denote  $r_i = r_i(\boldsymbol{\theta})$  for succinctness. MCME is an approximate ML estimator under conditions:

- i) For any true inliers, i.e.  $\forall i \in I^*$ ,  $r_i$  follows a zero-mean exponential distribution (from the natural exponential family) as  $r_i \sim \mathcal{N}(0, \sigma_i) = \exp(-\Phi(r_i, \sigma_i))$  for some scale parameter  $\sigma_i > 0$ , where  $\Phi$  is an increasing function of  $r_i$  on  $[0, +\infty)$ .
- ii) For any true outliers, i.e.  $\forall i \in \Omega \setminus I^*$ ,  $r_i$  follows a uniform distribution on the interval  $[\tau, u]$ , where  $u$  is the possible maximal perturbation of outliers.

*Proof:* Let  $P \in (0, 1]$  and  $(1 - P) \in [0, 1)$  denote the probability of inliers and outliers, respectively. Under conditions i) and ii), the likelihood of  $\mathbf{r} = [r_1, r_2, \dots, r_N]^T$  is given by

$$\mathcal{L}(\mathbf{r}; \boldsymbol{\theta}) = \prod_{i=1}^N [P \exp(-\Phi(r_i, \sigma_i))]^{1 - \mathbb{I}(\tau < r_i \leq u)} \times \left[ P \exp(-\Phi(r_i, \sigma_i)) + \frac{1 - P}{u - \tau} \right]^{\mathbb{I}(\tau < r_i \leq u)}.$$

The corresponding log-likelihood is

$$\begin{aligned} \log \mathcal{L}(\mathbf{r}; \boldsymbol{\theta}) &= \sum_{i=1}^N (1 - \mathbb{I}(\tau < r_i \leq u)) [-\Phi(r_i, \sigma_i) + \log P] \\ &\quad + \underbrace{\mathbb{I}(\tau < r_i \leq u) \log \left[ P \exp(-\Phi(r_i, \sigma_i)) + \frac{1 - P}{u - \tau} \right]}_{L_o(r_i)}. \end{aligned} \quad (6)$$

Since  $\Phi$  is an increasing function, for  $r_i \in (\tau, u]$  it follows that

$$\log(1 - P) - \log(u - \tau) < L_o(r_i) < L_o(\tau).$$

That is as  $r_i$  increases on  $(\tau, u]$ ,  $L_o(r_i)$  decreases from  $L_o(\tau)$  toward  $\log(1 - P) - \log(u - \tau)$ . Meanwhile, for sufficiently large  $u$ , we have  $\exp(-\Phi(r_i, \sigma_i)) \rightarrow 0$  for  $r_i > u$ . Hence, the likelihood is dominated by the two cases of  $r_i \leq \tau$  and  $\tau < r_i \leq u$ , i.e.,  $r_i \leq u$ . Then, from the fact that  $\mathbb{I}(\tau < r_i \leq u)$  is equivalent to  $\mathbb{I}(\Phi(\tau) < \Phi(r_i) \leq \Phi(u))$ , it is easy to see that with some  $\beta$  satisfying  $\log(1 - P) - \log(u - \tau) \leq \beta \leq L_o(\tau)$ , the minimization problem

$$\min_{\boldsymbol{\theta} \in \mathbb{R}^d, s_i \in \{0,1\}} \sum_{i=1}^N (1 - s_i)\Phi(r_i, \sigma_i) + \beta s_i,$$

can be viewed as an approximation of maximizing the log-likelihood (6). Under i.i.d assumption of inliers with  $\sigma_i = \sigma$  for  $\forall i \in I^*$ , taking the scale parameter  $\sigma$  into  $\beta$ , and ignoring constant terms independent on  $r_i$ , it leads to the MCME formulation (3).

*Remark 2.* The natural exponential family includes a large class of distributions. A special example is the Gaussian distribution, for which with zero-mean it has  $\Phi(r_i, \sigma_i) = \frac{r_i^2}{2\sigma_i^2} + \frac{1}{2} \log(2\pi\sigma_i^2)$ . This proposition indicates that MCME is an approximate ML estimator under the conditions that, the inlier noise is small and follows a natural exponential distribution, while the outliers contain large perturbation following a uniform distribution.

## B. Comparison between MC and MCME

This subsection compares MC with MCME to show that they can produce the same inlier set (hence be equivalent in this sense) in special conditions, but not in general conditions. Particularly, MCME has lower fitting residual than MC robust fitting.

Before proceeding to the results, we present some definitions will be used in the analysis. Denote

$$\boldsymbol{\theta}_I := \arg \min_{\boldsymbol{\theta} \in \mathbb{R}^d} \sum_{i \in I} \Phi(r_i(\boldsymbol{\theta})), \quad R(I) := \sum_{i \in I} \Phi(r_i(\boldsymbol{\theta}_I)),$$

and the objective of MCME as

$$f(\boldsymbol{\theta}, \mathbf{s}) := \sum_{i=1}^N (1 - s_i)\Phi(r_i(\boldsymbol{\theta})) + \Phi(\tau)s_i.$$

From Proposition 1, a solution of MCME with identified inlier set  $I$  must satisfies  $\Phi(r_i(\boldsymbol{\theta}_I)) \leq \Phi(\tau)$  for  $\forall i \in I$  and  $\Phi(r_i(\boldsymbol{\theta}_I)) > \Phi(\tau)$  for  $\forall i \in \Omega \setminus I$ . Accordingly, we define a set of all possible inlier sets associated with feasible solutions of MCME as

$$F := \{I : \Phi(r_i(\boldsymbol{\theta}_I)) \leq \Phi(\tau), \forall i \in I; \Phi(r_i(\boldsymbol{\theta}_I)) > \Phi(\tau), \forall i \in \Omega \setminus I; I \subseteq \Omega\}.$$

For any  $I \subseteq \Omega$ ,  $(\boldsymbol{\theta}_I, \mathbf{s}_I)$  is a feasible solution of MCME only when  $I \in F$ , where  $\mathbf{s}_I$  is a binary vector associated with  $I$  as

$$\mathbf{s}_I := [\mathbb{I}(1 \notin I), \mathbb{I}(2 \notin I), \dots, \mathbb{I}(N \notin I)]^T.$$

The following result gives a sufficient condition under which the two criterions produce the same consensus set.

*Proposition 3.* Suppose that  $\beta = \Phi(\tau)$ , and  $\Phi$  is increasing on  $[0, +\infty)$  with  $\Phi(0) = 0$ . Let  $I^*$  denote a solution of MC, and  $I^+$  denote the inlier set of a MCME solution, then,  $I^+$  is a consensus set and  $|I^+| \leq |I^*|$ . Furthermore, if  $\Phi(r_i(\boldsymbol{\theta}_{I^*})) \leq \Phi(\tau)$ ,  $\forall i \in I^*$ , and for any other consensus set  $I^\bullet \in F$  there holds

$$|I^*| - |I^\bullet| > (R(I^*) - R(I^\bullet))/\Phi(\tau), \quad (7)$$

then  $I^+ = I^*$ .

*Proof:* First, with  $\beta = \Phi(\tau)$ , it follows from (3) and Proposition 1 that any inlier set  $I^+$  produced by MCME satisfies  $\Phi(r_i(\boldsymbol{\theta}_{I^+})) \leq \Phi(\tau)$  for  $\forall i \in I^+$ . As  $\Phi$  is increasing on  $[0, +\infty)$ ,  $\Phi(r_i(\boldsymbol{\theta}_{I^+})) \leq \Phi(\tau)$  is equivalent to  $r_i(\boldsymbol{\theta}_{I^+}) \leq \tau$ . Thus,  $I^+$  must be a consensus set satisfies  $r_i(\boldsymbol{\theta}) \leq \tau$ ,  $\forall i \in I^+$  for some  $\boldsymbol{\theta}$ . Furthermore, since  $I^*$  is the maximum

consensus set, the size of  $I^+$  is upper bounded by the size of  $I^*$ , i.e.  $|I^+| \leq |I^*|$ . Under condition  $\Phi(r_i(\boldsymbol{\theta}_{I^*})) \leq \Phi(\tau)$ ,  $\forall i \in I^*$ , since  $I^*$  is a maximum consensus set, it follows that  $r_i(\boldsymbol{\theta}_{I^*}) > \tau$  and hence  $\Phi(r_i(\boldsymbol{\theta}_{I^*})) > \Phi(\tau)$  for  $\forall i \in \Omega \setminus I^*$ , otherwise there exists another consensus set  $I'$  such that  $I^* \subset I'$  and  $|I^*| < |I'|$ . Thus,  $I^* \in F$  and  $f(\boldsymbol{\theta}_{I^*}, \mathbf{s}_{I^*}) = R(I^*) + |\Omega \setminus I^*| \Phi(\tau)$ . Moreover, for a consensus set  $I^\bullet$  satisfying  $I^\bullet \in F$ , which is a necessary condition for  $I^\bullet$  to be the inlier set of a feasible MCME solution,  $f(\boldsymbol{\theta}_{I^\bullet}, \mathbf{s}_{I^\bullet}) = R(I^\bullet) + |\Omega \setminus I^\bullet| \Phi(\tau)$ . Then, for any such consensus set  $I^\bullet \neq I^*$  if it holds  $f(\boldsymbol{\theta}_{I^\bullet}, \mathbf{s}_{I^\bullet}) > f(\boldsymbol{\theta}_{I^*}, \mathbf{s}_{I^*})$ ,  $(\boldsymbol{\theta}_{I^*}, \mathbf{s}_{I^*})$  is a solution of MCME which attains the minimum objective value, and the corresponding inlier set is given by  $I^*$ . This inequality condition holds if  $R(I^\bullet) - |I^\bullet| \Phi(\tau) > R(I^*) - |I^*| \Phi(\tau)$ , which is equivalent to the condition (7).

*Remark 3.* As  $I^*$  is the largest consensus set, it follows that  $|I^*| \geq |I^\bullet|$  for any other consensus set  $I^\bullet$ . Then, it is easy to see that, with selection  $\beta = \Phi(\tau)$ , a condition for MCME to yield the same inlier set as MC is that the residual over  $I^*$  is very small (or relatively small compared with the residual over any  $I^\bullet$ ) and the condition  $\Phi(r_i(\boldsymbol{\theta}_{I^*})) \leq \Phi(\tau)$  for  $\forall i \in I^*$  is satisfied. However, they do not produce the same consensus set in general condition.

As MCME takes the inlier residual distribution of model fitting into account, while MC does not, a natural question arises: *Is MCME theoretically superior over MC?* Next we answer this question by comparing the lowest achievable residual of the two criterions.

*Theorem 4.* Let  $I^+$  denote the inlier set of an MCME solution and  $I^*$  denote a solution of MC. Suppose that  $\Phi$  is monotone increasing on  $[0, +\infty)$  with  $\Phi(0) = 0$ . Then, with  $\beta = \Phi(\tau)$ , the lowest achievable residual of MCME is lower than that of MC as

$$\min_{\boldsymbol{\theta} \in \mathbb{R}^d} \sum_{i \in I^+} \Phi(r_i(\boldsymbol{\theta})) \leq \min_{\boldsymbol{\theta} \in \mathbb{R}^d} \sum_{i \in I^*} \Phi(r_i(\boldsymbol{\theta})). \quad (8)$$

Furthermore, if  $I^* \notin F$ , the inequality in (8) holds strictly.

*Proof:* We consider two cases of the maximum consensus set  $I^*$  and prove Theorem 4 by contradiction.

*Case 1:*  $\Phi(r_i(\boldsymbol{\theta}_{I^*})) \leq \Phi(\tau)$ ,  $\forall i \in I^*$ . Similar to the argumentation in proving Proposition 3, in this case  $I^* \in F$  and  $(\boldsymbol{\theta}_{I^*}, \mathbf{s}_{I^*})$  is a feasible solution of MCME with objective value  $f(\boldsymbol{\theta}_{I^*}, \mathbf{s}_{I^*}) = R(I^*) + |\Omega \setminus I^*| \Phi(\tau)$ . Meanwhile, from Proposition 3, we have  $|I^+| \leq |I^*|$  and hence  $|\Omega \setminus I^+| \geq |\Omega \setminus I^*|$ . As  $I^+$  is the inlier set of an MCME solution, hence  $I^+ \in F$ . Then, if (8) does not hold, which implies  $R(I^+) > R(I^*)$  and further

$$\begin{aligned} f(\boldsymbol{\theta}_{I^+}, \mathbf{s}_{I^+}) &= R(I^+) + |\Omega \setminus I^+| \Phi(\tau) \\ &> R(I^*) + |\Omega \setminus I^*| \Phi(\tau) = f(\boldsymbol{\theta}_{I^*}, \mathbf{s}_{I^*}). \end{aligned}$$

This inequality means that if (8) does not hold, the feasible solution  $(\boldsymbol{\theta}_{I^*}, \mathbf{s}_{I^*})$  attains a lower objective value of MCME than  $(\boldsymbol{\theta}_{I^+}, \mathbf{s}_{I^+})$ . Obviously, it contradicts to that  $I^+$  is the inlier set of an MCME solution, under which  $(\boldsymbol{\theta}_{I^+}, \mathbf{s}_{I^+})$  should attain the minimum objective value of MCME.

*Case 2:* For some  $\hat{I}^* \subset I^*$ ,  $\Phi(r_i(\boldsymbol{\theta}_{\hat{I}^*})) \leq \Phi(\tau)$ ,  $\forall i \in \hat{I}^*$  and  $\Phi(r_i(\boldsymbol{\theta}_{I^*})) > \Phi(\tau)$ ,  $\forall i \in I^* \setminus \hat{I}^*$ . In this case, though  $I^*$  is a consensus set, it no longer holds that  $\Phi(r_i(\boldsymbol{\theta}_{I^*})) > \Phi(\tau)$

for  $\forall i \in \Omega \setminus I^*$ , and  $(\boldsymbol{\theta}_{I^*}, \mathbf{s}_{I^*})$  is no longer a feasible solution of MCME, i.e.  $I^* \notin F$ , there must exist another consensus set  $I' \in F$  such that  $(\boldsymbol{\theta}_{I'}, \mathbf{s}_{I'})$  attains a lower objective value of MCME than  $(\boldsymbol{\theta}_{I^*}, \mathbf{s}_{I^*})$  as  $R(I^*) + |\Omega \setminus I^*| \Phi(\tau) > R(I') + |\Omega \setminus I'| \Phi(\tau)$ . If (8) does not hold strictly, i.e.  $R(I^+) \geq R(I^*)$ , then, with  $|I^+| \leq |I^*|$ , it follows that

$$\begin{aligned} f(\boldsymbol{\theta}_{I^+}, \mathbf{s}_{I^+}) &= R(I^+) + |\Omega \setminus I^+| \Phi(\tau) \\ &\geq R(I^*) + |\Omega \setminus I^*| \Phi(\tau) \\ &> R(I') + |\Omega \setminus I'| \Phi(\tau) = f(\boldsymbol{\theta}_{I'}, \mathbf{s}_{I'}), \end{aligned}$$

which implies that there exists another feasible solution  $(\boldsymbol{\theta}_{I'}, \mathbf{s}_{I'})$  that can attain a lower objective value of MCME than  $(\boldsymbol{\theta}_{I^+}, \mathbf{s}_{I^+})$ . Obviously, it contradicts to that  $I^+$  is the inlier set of an MCME solution with  $(\boldsymbol{\theta}_{I^+}, \mathbf{s}_{I^+})$  attaining the minimum objective value of MCME. Thus, when  $I^* \notin F$ , the inequality in (8) holds strictly.

*Remark 4.* This theorem sheds some light on the superiority of MCME over MC in terms of the lowest achievable residual in model fitting. This advantage comes from the fact that, MCME with a single-step model fitting procedure takes the fitting residual and inlier distribution into consideration in identifying the inlier set, while MC does not.

### III. EFFECTIVE AND EFFICIENT ALGORITHM BASED ON SEMIDEFINITE RELAXATION

The MCME formulation (3) is not essentially any easier than the MC problem. It is also NP-hard, for which a global optimum can only be guaranteed by searching based algorithms. Though both formulations are intrinsically combinatorial problems, the unconstrained formulation of MCME facilitates us to develop effective deterministic non-global algorithm based on SDR. SDR has been shown to be very effective in handling combinatorial problems, and it is tighter than linear relaxation [24, 25]. Hence, it can be expected to achieve better performance than existing non-global deterministic MC algorithms. Note that, unlike most well-studied SDR problems resulting in convex relaxed formulations, the SDR of MCME is still nonconvex. However, it becomes biconvex in certain conditions, which we solve by an alternating convex search (ACS) algorithm.

#### A. Semidefinite Relaxation of the Binary Variable

We solve the MCME problem (3) via alternately updating the model parameter  $\boldsymbol{\theta}$  and the binary slack variable  $\mathbf{s}$ . Let  $\tilde{\mathbf{s}} \in \{-1, 1\}^{N+1}$ ,  $\mathbf{S} = \tilde{\mathbf{s}}\tilde{\mathbf{s}}^T$ ,  $\Phi_i := \Phi(r_i(\boldsymbol{\theta}))$ , and

$$\mathbf{\Lambda} = \begin{bmatrix} 0 & (\beta - \boldsymbol{\Phi}^T)/2 \\ (\beta - \boldsymbol{\Phi})/2 & \text{diag}(\boldsymbol{\Phi}) \end{bmatrix},$$

with  $\boldsymbol{\Phi} = [\Phi_1, \Phi_2, \dots, \Phi_N]^T$ . Then, the MCME problem is equivalent to

$$\min_{\boldsymbol{\theta} \in \mathbb{R}^d, \mathbf{S} \in \mathbb{S}^{(N+1)}} \text{tr}(\mathbf{\Lambda}\mathbf{S}) \quad (9)$$

subject to  $\text{diag}(\mathbf{S}) = \mathbf{1}_{N+1}$ ,  $\mathbf{S} \succeq \mathbf{0}$ ,  $\text{rank}(\mathbf{S}) = 1$ .

To justify this, firstly problem (3) can be rewritten as

$$\min_{\boldsymbol{\theta} \in \mathbb{R}^d, \mathbf{s} \in \{-1, 1\}^N} \sum_{i=1}^N (\beta - \Phi_i) s_i + \Phi_i s_i^2, \quad (10)$$

where we have changed  $\mathbf{s} \in \{0, 1\}^N$  to  $\mathbf{s} \in \{-1, 1\}^N$  for convenience. Then, the objective in (10) can be expressed as  $\tilde{\mathbf{s}}^T \mathbf{A} \tilde{\mathbf{s}}$  with  $\tilde{\mathbf{s}} = [t, \mathbf{s}^T]^T \in \{-1, 1\}^{N+1}$ . Here an auxiliary variable  $t \in \{-1, 1\}$  is introduced, with which  $\mathbf{s}/t$  will be the solution of the original problem (3). Using the relation that  $\mathbf{S} = \tilde{\mathbf{s}} \tilde{\mathbf{s}}^T$  with  $\tilde{\mathbf{s}} \in \{-1, 1\}^{N+1}$  is equivalent to  $\text{diag}(\mathbf{S}) = \mathbf{1}_{N+1}$ ,  $\mathbf{S} \succeq \mathbf{0}$  and  $\text{rank}(\mathbf{S}) = 1$ , problem (3) can be reformulated as (9).

Then, dropping the rank-1 nonconvex constraint leads to a SDR of (3) as

$$\begin{aligned} & \min_{\boldsymbol{\theta} \in \mathbb{R}^d, \mathbf{S} \in \mathcal{S}^{(N+1)}} \text{tr}(\mathbf{A}\mathbf{S}) \\ & \text{subject to } \text{diag}(\mathbf{S}) = \mathbf{1}_{N+1}, \quad \mathbf{S} \succeq \mathbf{0}. \end{aligned} \quad (11)$$

The above SDR is standard and widely used in binary combinatorial optimization problems [25], except that our problem additionally involves another variable  $\boldsymbol{\theta}$  needing to be solved simultaneously. As a consequence, unlike most existing well-studied SDR problems resulting in convex relaxed formulations, problem (11) is nonconvex. However, under mild condition that  $\Phi$  and  $r_i$  are convex, problem (11) is biconvex.

*Proposition 5.* If  $\Phi$  and  $r_i$  are convex, and  $\mathbf{S}(1, 2 : N+1) \leq 1$ , then problem (11) is biconvex in  $\boldsymbol{\theta}$  and  $\mathbf{S}$ .

This assertion is easy to justify. On one hand, if fixing  $\boldsymbol{\theta}$ , problem (11) is a standard semidefinite programming (SDP). On the other hand, if fixing  $\mathbf{S}$ , problem (11) becomes

$$\min_{\boldsymbol{\theta} \in \mathbb{R}^d} \sum_{i=1}^N (1 - S_{1,i+1}) \Phi(r_i(\boldsymbol{\theta})), \quad (12)$$

which is convex in  $\boldsymbol{\theta}$  when  $\Phi$  and  $r_i$  are convex and  $\mathbf{S}(1, 2 : N+1) \leq 1$ . Note that, when  $\Phi$  and  $r_i$  are convex,  $\mathbf{S}(1, 2 : N+1) \leq 1$  is a sufficient condition for (12) to be convex but not necessary. This sufficient condition can be guaranteed by adding  $\mathbf{S}(1, 2 : N+1) \leq 1$  or  $\mathbf{S} \leq 1$  into (9) as a redundant constraint. However, it is unnecessary in practice, since the SDP solution  $\mathbf{S}$  approximately has element values of  $\pm 1$ , though not exactly. In this scenario, (12) would be convex under non-degenerate condition. The convexity assumption of  $\Phi$  and  $r_i$  are naturally satisfied in most computer vision applications. For example, linear forms of  $r_i(\boldsymbol{\theta})$  are usually used in projective transformation in multi-view geometry, as will be shown in Section 4. Meanwhile, from the underlying mechanism of the MCME formulation, only measurements with small residuals are taken into account in computing  $\boldsymbol{\theta}$  through minimizing the loss  $\Phi$ . Hence, it is unnecessary to use a nonconvex robust loss and  $\Phi$  can be simply selected as the least-squares (LS) loss.

### B. Fast Algorithm for $\mathbf{S}$ -Update

Fixing  $\boldsymbol{\theta}$ , the  $\mathbf{S}$ -update subproblem becomes

$$\begin{aligned} & \min_{\mathbf{S} \in \mathcal{S}^{(N+1)}} \text{tr}(\mathbf{A}\mathbf{S}) \\ & \text{subject to } \text{diag}(\mathbf{S}) = \mathbf{1}_{N+1}, \quad \mathbf{S} \succeq \mathbf{0}. \end{aligned} \quad (13)$$

It is a standard SDP and can be solved by well-established SDP solvers, such as CVX [32]. But such solvers using primal-dual interior algorithm have a complexity of  $O((N+1)^{4.5})$  at the worst-case, and do not scale to moderate to large problem sizes.

In order to make the algorithm scalable to high dimension problems, the low-rank property of  $\mathbf{S}$  can be exploited by using a low-rank factorization  $\mathbf{S} = \mathbf{R}\mathbf{R}^T$  with  $\mathbf{R} \in \mathbb{R}^{(N+1) \times p}$  to recast (13) into [25]

$$\begin{aligned} & \min_{\mathbf{R} \in \mathbb{R}^{(N+1) \times p}} \text{tr}(\mathbf{A}\mathbf{R}\mathbf{R}^T) \\ & \text{subject to } \text{diag}(\mathbf{R}\mathbf{R}^T) = \mathbf{1}_{N+1}. \end{aligned} \quad (14)$$

With this reformulation, the parameter number is reduced from  $(N+1)^2$  to  $p(N+1)$ . It has been proven that there exists an optimum of (13) with rank less than  $\lceil \sqrt{2N} \rceil$  [33, 25], hence using  $p \geq \lceil \sqrt{2N} \rceil$  can guarantee that any optimum of (14) is also an optimum of (13). Meanwhile, although problem (14) is nonconvex, it almost never has any spurious local optima [34].

*Proposition 6 [34].* For almost all  $\mathbf{A}$ , if  $p(p+1) \geq 2(N+1)$ , any local optimum  $\mathbf{R}^\bullet$  of (14) is a global optimum of (14), and  $\mathbf{R}^\bullet \mathbf{R}^{\bullet T}$  is a global optimum of (13).

This result implies that, despite the nonconvexity of (14), local optimization algorithms can converge to global optima. Accordingly, the first-order augmented Lagrangian algorithm [25] can be used. Rather than directly using this algorithm, we exploit the sparsity structure of the problem to achieve further acceleration. This is based on the fact that only the first column, first row and diagonal of  $\mathbf{A}$  have nonzero elements. Specifically, let  $\mathbf{r}_i^T := \mathbf{R}(i, :)$  denote the  $i$ -th row of  $\mathbf{R}$  and  $\mathbf{r} := [\mathbf{r}_1^T, \mathbf{r}_2^T, \dots, \mathbf{r}_{N+1}^T]^T \in \mathbb{R}^{p(N+1)}$ , using the equivalence between  $\text{diag}(\mathbf{R}\mathbf{R}^T) = \mathbf{1}_{N+1}$  and  $\|\mathbf{r}_i\|^2 = 1$  for  $1 \leq i \leq N+1$ , problem (14) can be reformulated as an unconstrained problem

$$\min_{\mathbf{r} \in \mathbb{R}^{p(N+1)}} J(\mathbf{r}) := 2 \sum_{i=2}^{N+1} \Lambda_{1,i} \frac{\mathbf{r}_1^T \mathbf{r}_i}{\|\mathbf{r}_1\| \|\mathbf{r}_i\|} \quad (15)$$

where the norm-one constraints are removed by changing variable to  $[\mathbf{R}(i, :)]^T = \mathbf{r}_i / \|\mathbf{r}_i\|$  [35], which leads to an unconstrained formulation.

Due to the equivalence between (14) and (15), and from Proposition 6, a local optimization algorithm can be employed to solve (15), and any solution satisfies first- and second-order necessary optimality conditions is a global optimum. Hence, any efficient first-order algorithm can be employed, e.g., the limited memory BFGS (L-BFGS) algorithm [36]. Such algorithms only require evaluating the first-order gradient of the objective, which is

$$\nabla_{\mathbf{r}} J(\mathbf{r}) = \left[ \nabla_{\mathbf{r}_1^T} J(\mathbf{r}), \nabla_{\mathbf{r}_2^T} J(\mathbf{r}), \dots, \nabla_{\mathbf{r}_{N+1}^T} J(\mathbf{r}) \right]^T,$$

with

$$\begin{aligned} \nabla_{\mathbf{r}_1} J(\mathbf{r}) &= 2 \sum_{i=2}^{N+1} \Lambda_{1,i} \frac{\|\mathbf{r}_1\|^2 \mathbf{r}_i - \mathbf{r}_1^T \mathbf{r}_i \mathbf{r}_1}{\|\mathbf{r}_1\|^3 \|\mathbf{r}_i\|}, \\ \nabla_{\mathbf{r}_i} J(\mathbf{r}) &= 2 \Lambda_{1,i} \frac{\|\mathbf{r}_i\|^2 \mathbf{r}_1 - \mathbf{r}_1^T \mathbf{r}_i \mathbf{r}_i}{\|\mathbf{r}_1\| \|\mathbf{r}_i\|^3}, \quad \text{for } 2 \leq i \leq N+1. \end{aligned}$$

### C. $\boldsymbol{\theta}$ -Update

For fixing  $\mathbf{S}$ , the  $\boldsymbol{\theta}$ -subproblem is given by (12), which depends on the residual models of specific applications. We consider two main cases, linear or nonlinear residual model.

*Case 1 (Linear residual).* Linear residual model is widely used in MC [1], which typically has a form of

$$r_i(\boldsymbol{\theta}) = |\mathbf{a}_i^T \boldsymbol{\theta} - b_i|. \quad (16)$$

In robust linear regression and many computer vision applications, the residual  $r_i(\boldsymbol{\theta})$  can be conveniently expressed in this form. As will be shown in Section 4, in homography, fundamental matrix, and affinity estimation in multi-view geometry under algebraic distance, the residual can be expressed in a linear form as (16). With linear residual model, if  $\Phi$  is chosen as the LS loss, the model fitting term in MCME becomes

$$\Phi(r_i(\boldsymbol{\theta})) = (\mathbf{a}_i^T \boldsymbol{\theta} - b_i)^2. \quad (17)$$

Then, the  $\boldsymbol{\theta}$ -subproblem is quadratic and can be solved explicitly. In this case, a sufficient and necessary condition for the  $\boldsymbol{\theta}$ -subproblem (12) to be convex, under which problem (11) is biconvex, is

$$\sum_{i=1}^N (1 - S_{1,i+1}) \mathbf{a}_i \mathbf{a}_i^T \succeq \mathbf{0},$$

which is relaxed to  $\mathbf{S}(1, 2 : N + 1) \leq 1$  in Proposition 6.

Note that, even with quasi-convex geometric distance, deterministic MC algorithms usually use linear residual model, as both the  $\ell_1$ - and  $\ell_\infty$ -norm reprojection residual under geometric distance can be linearized, e.g., in homography estimation and triangulation. However, we handle it in a different manner as presented in the following *Case 2*. Moreover, in rotation search, additional norm-one constraint appears under the linear residual model, which can also be solved explicitly as detailed in Section 4.3.

*Case 2 (Nonlinear residual).* Geometric distance based residual model is geometrically or statistically meaningful and, hence, is of more interested in practical applications than algebraic distance [37]. For many vision applications, the geometric residual functions have a generalized form as [37], [38]

$$r_i(\boldsymbol{\theta}) = \frac{\|\mathbf{U}_i \boldsymbol{\theta} + \mathbf{u}_i\|_p}{\mathbf{w}_i^T \boldsymbol{\theta} + w_i}, \quad \text{with} \quad \mathbf{w}_i^T \boldsymbol{\theta} + w_i > 0, \quad (18)$$

where  $p \geq 1$ ,  $\mathbf{U}_i \in \mathbb{R}^{2 \times d}$ ,  $\mathbf{u}_i \in \mathbb{R}^2$ , and  $\mathbf{w}_i \in \mathbb{R}^d$ . In MC methods, linearization is usually used to handle such quasi-convex residual. For example, with a residual threshold of  $\tau$  (in geometric unit such as pixel), the residual constraint can be expressed as

$$\|\mathbf{U}_i \boldsymbol{\theta} + \mathbf{u}_i\|_p \leq \tau (\mathbf{w}_i^T \boldsymbol{\theta} + w_i), \quad (19)$$

where  $\mathbf{w}_i^T \boldsymbol{\theta} + w_i > 0$  is implicitly satisfied since  $\tau > 0$  and  $\|\mathbf{U}_i \boldsymbol{\theta} + \mathbf{u}_i\|_p \geq 0$ . Then, for the two special cases of  $p = 1$  or  $p = \infty$ , corresponding to the  $\ell_1$ - and  $\ell_\infty$ -norm, respectively, (19) can be equivalently expressed as four linear inequalities.

Naturally, for the MCME method, we can use the squared  $\ell_2$  reprojection error as the individual loss, i.e.,

$$\Phi(r_i(\boldsymbol{\theta})) = \frac{\|\mathbf{U}_i \boldsymbol{\theta} + \mathbf{u}_i\|^2}{(\mathbf{w}_i^T \boldsymbol{\theta} + w_i)^2}. \quad (20)$$

Then, gradient descent based algorithm can be directly applied to update  $\boldsymbol{\theta}$ . Alternatively, the  $\ell_\infty$  approach [39], [40] can be

---

**Algorithm 1:** Alternating Convex Search (ACS) Algorithm

---

**Input:** A start point  $(\boldsymbol{\theta}_0, \mathbf{S}_0)$ , and set  $\beta > 0$ .

**While** not converged ( $k = 0, 1, 2, \dots$ ) **do**

Solve the SDP (13) for fixed  $\boldsymbol{\theta}_k$  to obtain  $\mathbf{S}^*$  and set  $\mathbf{S}_{k+1} = \mathbf{S}^*$ .

Solve the  $\boldsymbol{\theta}$ -subproblem for fixed  $\mathbf{S}_{k+1}$  to obtain  $\boldsymbol{\theta}^*$  and set

$\boldsymbol{\theta}_{k+1} = \boldsymbol{\theta}^*$ .

**End while**

**Output:**  $(\boldsymbol{\theta}_{k+1}, \mathbf{S}_{k+1})$ .

---

adopted, which minimizes the  $\ell_\infty$ -norm of individual reprojection errors instead of the sum of their square. As the point-wise maximum (equivalently the  $\ell_\infty$ -norm) of a set of quasi-convex functions is still quasi-convex, it does not have local minima. In comparison, the sum of quasi-convex functions (20) is no longer quasi-convex and can have multiple local minima.

#### D. Convergence of the ACS Algorithm

The ACS algorithm is summarized in Algorithm 1. The convergence properties of the ACS algorithm for biconvex minimization have been well established [41]. It has been shown that under weak conditions, the set of accumulation points generated by ACS form a connected, compact set and each of these points is a stationary point.

*Proposition 7 [41].* Denote the objective of (11) by  $f(\boldsymbol{\theta}, \mathbf{S})$ . Under the conditions in Proposition 5, the sequence  $\{f(\boldsymbol{\theta}_k, \mathbf{S}_k)\}_{k \in \mathbb{N}}$  generated by Algorithm 1 converges monotonically.

*Proposition 8 [41].* Under the conditions in Proposition 5, if the sequence  $\{(\boldsymbol{\theta}_k, \mathbf{S}_k)\}_{k \in \mathbb{N}}$  generated by Algorithm 1 is bounded, then the sequence has at least one accumulation point. Furthermore,

i) If for each accumulation point  $(\boldsymbol{\theta}^*, \mathbf{S}^*)$  the minimum solutions of both  $f(\boldsymbol{\theta}, \mathbf{S}^*)$  and  $f(\boldsymbol{\theta}^*, \mathbf{S})$  are unique, then  $\lim_{k \rightarrow \infty} \|\boldsymbol{\theta}_{k+1} - \boldsymbol{\theta}_k\| = 0$  and  $\lim_{k \rightarrow \infty} \|\mathbf{S}_{k+1} - \mathbf{S}_k\| = 0$ , and the accumulation points form a connected, compact set. Moreover, each accumulation point lies in the interior of the domain of  $f$  is a stationary point of  $f$ .

ii) If the sequence  $\{(\boldsymbol{\theta}_k, \mathbf{S}_k)\}_{k \in \mathbb{N}}$  converges to  $(\boldsymbol{\theta}^*, \mathbf{S}^*)$ , then  $(\boldsymbol{\theta}^*, \mathbf{S}^*)$  is a partial optimum such that  $f(\boldsymbol{\theta}^*, \mathbf{S}^*) \leq f(\boldsymbol{\theta}, \mathbf{S}^*)$ ,  $\forall \boldsymbol{\theta} \in \mathbb{R}^d$  and  $f(\boldsymbol{\theta}^*, \mathbf{S}^*) \leq f(\boldsymbol{\theta}^*, \mathbf{S})$ ,  $\forall \mathbf{S} \in \mathbb{S}^{N+1}$ .

Though these results still do not guarantee the global convergence of the whole sequence  $\{(\boldsymbol{\theta}_k, \mathbf{S}_k)\}_{k \in \mathbb{N}}$ , they are close enough for all practical purposes. Since the ACS algorithm is a local optimization algorithm, to reduce the probability of converging to a poor local minima, a proper initialization is useful for it to perform satisfactorily.

## IV. APPLICATIONS

This section presents the applications of MCME, mainly include projective transformation estimation in multi-view geometry under algebraic or geometric distance, rotation search, and 6-DoF rigid registration. Projective transformations and projections constitute a cornerstone of modern vision geometry [37]. Rotation search, also known as the Wahba problem, aims to estimate the rotation between two coordinate frames, which has wide applications in computer vision, robotics, and aerospace engineering [42]–[46]. 6-DoF rigid registration can

be viewed as an extension of 3-DoF rotation search, which estimates both rotation and translation.

### A. Projective Transformation Estimation with Algebraic Distance

This subsection applies the proposed method to homography, fundamental matrix and affinity estimation under algebraic distance. For all these problems, the set of correspondences from two views are denoted by  $\{(\mathbf{x}_i, \mathbf{x}'_i) : \mathbf{x}_i \leftrightarrow \mathbf{x}'_i, i = 1, 2, \dots, N\}$  with  $\mathbf{x}_i, \mathbf{x}'_i \in \mathbb{P}^2$ . Meanwhile,  $\tilde{\mathbf{x}}_i = [\mathbf{x}_i^T \ 1]^T$  and  $\tilde{\mathbf{x}'_i} = [\mathbf{x}'_i^T \ 1]^T$  are the homogeneous representation.

Homography arises in plane-to-plane mapping. The problem is to compute a matrix  $\mathbf{H} \in \mathbb{R}^{3 \times 3}$  such that  $\tilde{\mathbf{x}}_i = \mathbf{H}\tilde{\mathbf{x}'_i}$  for inliers. The matrix  $\mathbf{H}$  has 8 DoF and is only defined up to scale. Accordingly, it can be conveniently defined as

$$\mathbf{H} = \begin{bmatrix} h_1 & h_2 & h_3 \\ h_4 & h_5 & h_6 \\ h_7 & h_8 & 1 \end{bmatrix}.$$

Denote  $\boldsymbol{\theta} = [h_1, h_2, \dots, h_8]^T \in \mathbb{R}^8$ , homography estimation with algebraic distance can be expressed in a linear form as [37]

$$\mathbf{A}\boldsymbol{\theta} = \mathbf{b}, \quad (21)$$

where  $\mathbf{A} = [\mathbf{a}_1, \dots, \mathbf{a}_N]^T$  and  $\mathbf{b} = [b_1, \dots, b_N]^T$  are determined by  $\{(\mathbf{x}_i, \mathbf{x}'_i) : i = 1, 2, \dots, N\}$ . With this expression, linear residual model is usually used in MC as (16). Using linear residual and with  $\Phi$  being the LS loss, the model fitting term in MCME conforms to (17).

Fundamental matrix is the algebraic representation of intrinsic projective geometry between two views. The problem is to compute a matrix  $\mathbf{F} \in \mathbb{R}^{3 \times 3}$  such that  $\tilde{\mathbf{x}}_i^T \mathbf{F} \tilde{\mathbf{x}'_i} = 0$  for inliers. Though the reprojection error is neither linear nor quasi-convex, the epipolar constraint  $\tilde{\mathbf{x}}_i^T \mathbf{F} \tilde{\mathbf{x}'_i} = 0$  can be linearized to have a form of (21) with  $\boldsymbol{\theta} = \text{vec}(\mathbf{F}) \in \mathbb{R}^9$  [37].

Affinity estimation also admits a linear residual model, in which the geometric matching error for the  $i$ -th correspondence is

$$r_i(\boldsymbol{\theta}) = \|\mathbf{x}_i - \boldsymbol{\Theta}\tilde{\mathbf{x}'_i}\|_1,$$

where  $\boldsymbol{\Theta} \in \mathbb{R}^{2 \times 3}$  stands for the affine transformation, and  $\boldsymbol{\theta} = \text{vec}(\boldsymbol{\Theta}) \in \mathbb{R}^6$ . This residual can be split into two terms, which also conforms to (16). Particularly, for affine transformation, geometric and algebraic distances are identical.

### B. Projective Transformation Estimation with Geometric Distance

While algebraic distance is convenient due to its linearity, geometric distance is geometrically or statistically meaningful. Interested application examples include homography estimation and triangulation. For homography estimation, the geometric residual is given by

$$r_i(\boldsymbol{\theta}) = \frac{\|[\mathbf{h}_1, \mathbf{h}_2]^T \tilde{\mathbf{x}'_i} - \mathbf{h}_3^T \tilde{\mathbf{x}'_i} \mathbf{x}_i\|_p}{\mathbf{h}_3^T \tilde{\mathbf{x}'_i}},$$

where  $\mathbf{h}_k^T$  is the  $k$ -th row of  $\mathbf{H}$  and  $\boldsymbol{\theta} = \text{vec}(\mathbf{H})$ . Given multi-view observations of 3D points with known camera matrices,

the triangulation problem is to estimate the 3D points that project to the given image points. For triangulation, for each image point  $\mathbf{x}_i$  and camera matrix  $\mathbf{P}_i \in \mathbb{R}^{3 \times 4}$ , the reprojection error of the point estimation  $\boldsymbol{\theta} \in \mathbb{R}^3$  is

$$r_i(\boldsymbol{\theta}) = \frac{\|([\mathbf{p}_1^i, \mathbf{p}_2^i]^T - \mathbf{x}_i \mathbf{p}_3^{iT}) \tilde{\boldsymbol{\theta}}\|_p}{\mathbf{p}_3^{iT} \tilde{\boldsymbol{\theta}}},$$

where  $\mathbf{p}_k^{iT}$  is the  $k$ -th row of  $\mathbf{P}_i$  and  $\tilde{\boldsymbol{\theta}} = [\boldsymbol{\theta}^T \ 1]^T$ . In both the applications with geometric distance, the residual have a form of (18), and the proposed algorithm can be applied.

### C. Rotation Search

Consider a set of 3D point pairs  $\{(\mathbf{a}_i, \mathbf{b}_i) : i = 1, 2, \dots, N\}$  with  $\mathbf{a}_i, \mathbf{b}_i \in \mathbb{R}^3$ , which are generated as

$$\mathbf{b}_i = \mathbf{R}\mathbf{a}_i + \mathbf{n}_i + \mathbf{o}_i, \quad (22)$$

where  $\mathbf{R} \in \text{SO}(3)$  is an unknown rotation matrix,  $\mathbf{n}_i$  models small inlier measurement noise,  $\mathbf{o}_i$  is zero if the data pair  $(\mathbf{a}_i, \mathbf{b}_i)$  is inlier, or  $\mathbf{o}_i$  is an arbitrary perturbation if  $(\mathbf{a}_i, \mathbf{b}_i)$  is outlier.

For convenience, we adopt quaternion representation for 3D rotation [47]. Denote a unit quaternion by  $\mathbf{q} = [\mathbf{v}^T \ s]^T$ , where  $\mathbf{v} \in \mathbb{R}^3$  is the vector part and  $s$  is the scalar part. If  $\mathbf{R}$  is the unique rotation corresponding to a unit quaternion  $\mathbf{q}$ , then the rotation of a vector  $\mathbf{a} \in \mathbb{R}^3$  by  $\mathbf{R}$  can be expressed in terms of quaternion product as

$$\begin{bmatrix} \mathbf{R}\mathbf{a} \\ 0 \end{bmatrix} = \mathbf{q} \circ \hat{\mathbf{a}} \circ \mathbf{q}^{-1},$$

where  $\mathbf{q}^{-1} = [-\mathbf{v}^T \ s]^T$  is the quaternion inverse, and  $\hat{\mathbf{a}} = [\mathbf{a}^T \ 0]^T$ . The quaternion product is defined as  $\mathbf{q}_1 \circ \mathbf{x} = \Omega(\mathbf{q}_1)\mathbf{x}$  for any  $\mathbf{x} \in \mathbb{R}^4$ , and  $\mathbf{q}_1 \circ \mathbf{q}_2 = \Omega(\mathbf{q}_1)\mathbf{q}_2 = \bar{\Omega}(\mathbf{q}_2)\mathbf{q}_1$  for two unit quaternion  $\mathbf{q}_1$  and  $\mathbf{q}_2$ , where

$$\Omega(\mathbf{q}) = \begin{bmatrix} q_4 & -q_3 & q_2 & q_1 \\ q_3 & q_4 & -q_1 & q_2 \\ -q_2 & q_1 & q_4 & q_3 \\ -q_1 & -q_2 & -q_3 & q_4 \end{bmatrix}, \quad \bar{\Omega}(\mathbf{q}) = \begin{bmatrix} q_4 & q_3 & -q_2 & q_1 \\ -q_3 & q_4 & q_1 & q_2 \\ q_2 & -q_1 & q_4 & q_3 \\ -q_1 & -q_2 & -q_3 & q_4 \end{bmatrix}.$$

Based on quaternion representation, the linear residual with a LS loss can be expressed as

$$\Phi(r_i(\boldsymbol{\theta})) = \|\hat{\mathbf{b}}_i - \boldsymbol{\theta} \circ \hat{\mathbf{a}}_i \circ \boldsymbol{\theta}^{-1}\|^2, \quad \text{with } \|\boldsymbol{\theta}\| = 1. \quad (23)$$

Similar to (11), the SDR of MCME in this case leads to

$$\min_{\boldsymbol{\theta} \in \mathbb{R}^4, \mathbf{S} \in \mathbb{S}^{(N+1)}} \text{tr}(\boldsymbol{\Lambda}\mathbf{S}) \quad (24)$$

$$\text{subject to } \text{diag}(\mathbf{S}) = \mathbf{1}_{N+1}, \quad \mathbf{S} \succeq \mathbf{0}, \quad \|\boldsymbol{\theta}\| = 1.$$

Accordingly, the  $\boldsymbol{\theta}$ -subproblem becomes

$$\min_{\boldsymbol{\theta} \in \mathbb{R}^4} \sum_{i=1}^N (1 - S_{1,i+1}) \|\hat{\mathbf{b}}_i - \boldsymbol{\theta} \circ \hat{\mathbf{a}}_i \circ \boldsymbol{\theta}^{-1}\|^2 \quad (25)$$

$$\text{subject to } \|\boldsymbol{\theta}\| = 1.$$

For a unit quaternion  $\boldsymbol{\theta}$ , it follows that  $c = \boldsymbol{\theta}^T (c\mathbf{I}_4)\boldsymbol{\theta}$  for any  $c \in \mathbb{R}$ ,  $\hat{\mathbf{b}}_i^T(\boldsymbol{\theta} \circ \hat{\mathbf{a}}_i \circ \boldsymbol{\theta}^{-1}) = \boldsymbol{\theta}^T \Omega^T(\hat{\mathbf{b}}_i) \bar{\Omega}(\hat{\mathbf{a}}_i) \boldsymbol{\theta}$  and  $-\Omega^T(\hat{\mathbf{b}}_i) = \Omega(\hat{\mathbf{b}}_i)$ , hence problem (25) can be rewritten as

$$\min_{\boldsymbol{\theta} \in \mathbb{R}^4} \boldsymbol{\theta}^T \mathbf{G} \boldsymbol{\theta}, \quad \text{subject to } \|\boldsymbol{\theta}\| = 1, \quad (26)$$

with

$$\mathbf{G} = \sum_{i=1}^N (1 - \mathbf{S}_{1,i+1}) \left[ \left( \|\mathbf{b}_i\|^2 + \|\mathbf{a}_i\|^2 \right) \mathbf{I}_4 + 2\Omega(\hat{\mathbf{b}}_i)\bar{\Omega}(\hat{\mathbf{a}}_i) \right].$$

Obviously, the solution of (26) is given by the eigenvector corresponding to the smallest eigenvalue of  $\mathbf{G}$ .

Next, we compare the proposed method with a close existing method [31], namely QUASAR (QUaternion-based Semidefinite relAXation for Robust alignment). QUASAR uses a truncated LS loss and has a formulation as

$$\min_{\substack{\boldsymbol{\theta} \in \mathbb{R}^4, \|\boldsymbol{\theta}\|=1 \\ s_i \in \{-1,1\}}} \sum_{i=1}^N \frac{1-s_i}{2} \frac{\|\hat{\mathbf{b}}_i - \boldsymbol{\theta} \circ \hat{\mathbf{a}}_i \circ \boldsymbol{\theta}^{-1}\|^2}{\sigma^2} + \frac{1+s_i}{2} \bar{c}^2, \quad (27)$$

which can be viewed as a special instance of the MCME formulation. To solve this mixed-integer program, QUASAR adopts a binary cloning based reformulation as

$$\min_{\substack{\boldsymbol{\theta} \in \mathbb{R}^4, \|\boldsymbol{\theta}\|=1 \\ \theta_i = \pm \theta}} \sum_{i=1}^N \frac{\|\hat{\mathbf{b}}_i - \boldsymbol{\theta} \circ \hat{\mathbf{a}}_i \circ \boldsymbol{\theta}^{-1} - \boldsymbol{\theta}^T \theta_i \hat{\mathbf{b}}_i + \boldsymbol{\theta} \circ \hat{\mathbf{a}}_i \circ \boldsymbol{\theta}_i^{-1}\|^2}{4\sigma^2} + \frac{1 + \boldsymbol{\theta}^T \boldsymbol{\theta}_i}{2} \bar{c}^2. \quad (28)$$

This reformulation is based on the fact that, if  $\boldsymbol{\theta}_i = s_i \boldsymbol{\theta}$  with  $s_i \in \{-1, 1\}$ , then  $\boldsymbol{\theta}^T \boldsymbol{\theta}_i = s_i$  and  $\boldsymbol{\theta} \circ \hat{\mathbf{a}}_i \circ \boldsymbol{\theta}_i^{-1} = s_i (\boldsymbol{\theta} \circ \hat{\mathbf{a}}_i \circ \boldsymbol{\theta}^{-1})$ . Let  $\tilde{\boldsymbol{\theta}} = [\boldsymbol{\theta}^T, \boldsymbol{\theta}_1^T, \dots, \boldsymbol{\theta}_N^T]^T$ , problem (28) can be expressed as [31]

$$\min_{\tilde{\boldsymbol{\theta}} \in \mathbb{R}^{4(N+1)}} \tilde{\boldsymbol{\theta}}^T \mathbf{Q} \tilde{\boldsymbol{\theta}} \quad (29)$$

subject to  $\|\boldsymbol{\theta}\| = 1$ ,  $\boldsymbol{\theta}_i \boldsymbol{\theta}_i^T = \boldsymbol{\theta} \boldsymbol{\theta}^T$ ,  $\forall i = 1, \dots, N$ ,

where  $\mathbf{Q} \in \mathbb{R}^{4(N+1) \times 4(N+1)}$  is given by

$$\mathbf{Q} = \begin{bmatrix} \mathbf{0} & \mathbf{Q}_{01} & \cdots & \mathbf{Q}_{0N} \\ \mathbf{Q}_{01} & \mathbf{Q}_{11} & \cdots & \mathbf{0} \\ \vdots & \vdots & \ddots & \vdots \\ \mathbf{Q}_{0N} & \mathbf{0} & \cdots & \mathbf{Q}_{NN} \end{bmatrix},$$

with

$$\mathbf{Q}_{ii} = \frac{(\|\mathbf{b}_i\|^2 + \|\mathbf{a}_i\|^2) \mathbf{I}_4 + 2\Omega(\hat{\mathbf{b}}_i)\bar{\Omega}(\hat{\mathbf{a}}_i)}{2\sigma^2} + \frac{\bar{c}^2}{2} \mathbf{I}_4,$$

$$\mathbf{Q}_{0i} = -\frac{(\|\mathbf{b}_i\|^2 + \|\mathbf{a}_i\|^2) \mathbf{I}_4 + 2\Omega(\hat{\mathbf{b}}_i)\bar{\Omega}(\hat{\mathbf{a}}_i)}{4\sigma^2} + \frac{\bar{c}^2}{4} \mathbf{I}_4.$$

Then, let  $\mathbf{Z} = \tilde{\boldsymbol{\theta}} \tilde{\boldsymbol{\theta}}^T \in \mathbb{S}^{4(N+1)}$  and denote its  $4 \times 4$  sub-blocks by  $[\mathbf{Z}]_{ij} = \boldsymbol{\theta}_i \boldsymbol{\theta}_j^T$  for  $\forall 0 \leq i, j \leq N$  with  $\boldsymbol{\theta}_0 = \boldsymbol{\theta}$ , QUASAR adopts a SDR of (29) as

$$\begin{aligned} & \min_{\mathbf{Z} \in \mathbb{S}^{4(N+1)}} \text{tr}(\mathbf{Q}\mathbf{Z}) \\ & \text{subject to } \text{tr}([\mathbf{Z}]_{00}) = 1, \mathbf{Z} \succeq \mathbf{0}, \\ & [\mathbf{Z}]_{ii} = [\mathbf{Z}]_{00}, \forall i = 1, \dots, N, \\ & [\mathbf{Z}]_{ij} = [\mathbf{Z}]_{ij}^T, \forall 0 \leq i < j \leq N. \end{aligned} \quad (30)$$

The next result compares QUASAR with the proposed method.

*Proposition 9.* If the MCME formulation uses the loss (23) and with  $\beta = \sigma^2 \bar{c}^2$ , then it is equivalent to the QUASAR formulations (27)–(29). Furthermore, the relaxation (24) of MCME is tighter than the relaxation (30) of QUASAR.

*Proof:* When the loss (23) and  $\beta = \sigma^2 \bar{c}^2$  are used in MCME, it is easy to see the equivalence between (3) and (27) by changing variable from  $s_i \in \{0, 1\}$  to  $s_i \in \{-1, 1\}$ . To justify (24) is tighter than (30), we first show that

$$\text{tr}(\boldsymbol{\Lambda}\mathbf{S}) = 2\sigma^2 \text{tr} \left( \mathbf{Q} \left( \mathbf{S} \otimes (\boldsymbol{\theta} \boldsymbol{\theta}^T) \right) \right) - \sigma^2 \bar{c}^2. \quad (31)$$

From the properties of the trace and Kronecker product operations, some algebra leads to  $\text{tr} \left( \mathbf{Q} \left( \mathbf{S} \otimes (\boldsymbol{\theta} \boldsymbol{\theta}^T) \right) \right) = \boldsymbol{\theta}^T \bar{\mathbf{Q}} \boldsymbol{\theta}$  with

$$\bar{\mathbf{Q}} = \sum_{i=1}^N \mathbf{Q}_{ii} + 2\mathbf{S}_{1,i+1} \mathbf{Q}_{0i}.$$

Similarly, with the loss (23) and  $\beta = \sigma^2 \bar{c}^2$ , it follows that  $\text{tr}(\boldsymbol{\Lambda}\mathbf{S}) = 2\sigma^2 \boldsymbol{\theta}^T \bar{\mathbf{Q}} \boldsymbol{\theta} - \sigma^2 \bar{c}^2$ , which leads to (31). Hence, the relaxation (24) is equivalent to

$$\begin{aligned} & \min_{\boldsymbol{\theta} \in \mathbb{R}^4, \mathbf{S} \in \mathbb{S}^{(N+1)}} \text{tr} \left( \mathbf{Q} \left( \mathbf{S} \otimes (\boldsymbol{\theta} \boldsymbol{\theta}^T) \right) \right) \\ & \text{subject to } \|\boldsymbol{\theta}\| = 1, \text{diag}(\mathbf{S}) = \mathbf{1}_{N+1}, \mathbf{S} \succeq \mathbf{0}, \end{aligned}$$

which is further equivalent to

$$\begin{aligned} & \min_{\mathbf{Z} \in \mathbb{S}^{4(N+1)}} \text{tr}(\mathbf{Q}\mathbf{Z}) \\ & \text{subject to } [\mathbf{Z}]_{00} = \boldsymbol{\theta} \boldsymbol{\theta}^T, \|\boldsymbol{\theta}\| = 1, \\ & [\mathbf{Z}]_{ii} = [\mathbf{Z}]_{00}, \forall i = 1, \dots, N, \\ & [\mathbf{Z}]_{ij} = s_{ij} [\mathbf{Z}]_{00}, \forall 0 \leq i < j \leq N, \quad (32) \\ & \mathbf{S} = \begin{bmatrix} 1 & s_{01} & \cdots & s_{0N} \\ s_{01} & 1 & \cdots & s_{1N} \\ \vdots & \vdots & \ddots & \vdots \\ s_{0N} & s_{1N} & \cdots & 1 \end{bmatrix} \succeq \mathbf{0}. \end{aligned}$$

Then, it is easy to see that the constraints in (32) in fact constitute a subset of the constraints in (30). Hence, the optimum objective of (32) (equivalently that of (24)) provides a tighter lower bound to the original nonconvex problem than (30).

*Remark 4 (Comparison on computational complexity).* It has been shown in [31] that the relaxation (30) with redundant constraints is sufficiently tight. Particularly, in the noiseless and outlier-free case, it is always tight as its optimal solution has rank-1 and attains a global minimum of the original non-convex problem. However, QUASAR solving (30) is computationally expensive and scales poorly in problem size. For example, with a general SDP solver it typically needs more than 1000 seconds for  $N = 100$  [31]. Although (30) is also a SDP like the  $\mathbf{S}$ -subproblem (13), the accelerating procedure in Section 3.2 does not apply to it. That is because the SDP (30) involves a large number of equality constraints, about  $3N^2 + 13N$ . Meanwhile, the constraints do not admit an unconstrained formulation. Hence, when using the augmented Lagrangian method, a large number of dual variables (about  $3N^2 + 13N$ ) have to be handled, which fundamentally increases the computational complexity. In comparison, (13) only has  $N + 1$  equality constraints and, more importantly, the



norm-one constraints have a special “hidden convexity” structure admitting an unconstrained formulation (15). This leads to a significant advantage of our algorithm over QUASAR in computational efficiency, e.g., three orders of magnitude faster as will be shown in Section 5.5.

#### D. 6-DoF Euclidean Registration

In the context of 6-DoF Euclidean registration defined by a rigid transformation  $[\mathbf{R}, \mathbf{t}] \in \mathbb{R}^{3 \times 4}$ , where  $\mathbf{R} \in \text{SO}(3)$  and  $\mathbf{t}$  are the unknown rotation and translation, respectively, the generation model (22) is extended to

$$\mathbf{b}_i = \mathbf{R}\mathbf{a}_i + \mathbf{t} + \mathbf{n}_i + \mathbf{o}_i. \quad (33)$$

In this case, using quaternion representation for rotation and with the LS loss, the fitting objective becomes

$$\Phi(r_i(\boldsymbol{\theta})) = \left\| \hat{\mathbf{b}}_i - \boldsymbol{\theta} \circ \hat{\mathbf{a}}_i \circ \boldsymbol{\theta}^{-1} - \hat{\mathbf{t}} \right\|^2, \quad \text{with } \|\boldsymbol{\theta}\| = 1, \quad (34)$$

where  $\hat{\mathbf{t}} = [\mathbf{t}^T \ 0]^T$ . Accordingly, the  $\boldsymbol{\theta}$ -subproblem becomes

$$\min_{\boldsymbol{\theta} \in \mathbb{R}^4, \mathbf{t} \in \mathbb{R}^3} \sum_{i=1}^N (1 - S_{1,i+1}) \left\| \hat{\mathbf{b}}_i - \boldsymbol{\theta} \circ \hat{\mathbf{a}}_i \circ \boldsymbol{\theta}^{-1} - \hat{\mathbf{t}} \right\|^2 \quad (35)$$

subject to  $\|\boldsymbol{\theta}\| = 1$ .

Although this subproblem no longer admits a direct solution like (25), it can be efficiently solved via alternative minimization between  $\boldsymbol{\theta}$  and  $\mathbf{t}$ . Specifically, for fixed  $\mathbf{t}$  it degenerates to a form of (25) and the solution of  $\boldsymbol{\theta}$  can be directly obtained via eigen-decomposition, while for fixed  $\boldsymbol{\theta}$  the solution of  $\mathbf{t}$  is explicitly given by

$$\hat{\mathbf{t}} = \left[ \sum_{i=1}^N (1 - S_{1,i+1}) \right]^{-1} \sum_{i=1}^N (1 - S_{1,i+1}) \left( \hat{\mathbf{b}}_i - \boldsymbol{\theta} \circ \hat{\mathbf{a}}_i \circ \boldsymbol{\theta}^{-1} \right).$$

This alternating method can usually converge to a sufficient accuracy within a few iterations.

## V. EXPERIMENTAL RESULTS

We evaluate the proposed MCME method in various experiments, including robust linear regression, homography estimation, 3-DoF rotation registration, and 6-DoF Euclidean registration. The experiments are conducted on a desktop PC with a 3.4 GHz Intel Core I5-4670 CPU and 32 GB RAM. For MCME, we set  $p = \lceil \sqrt{2N}/3 \rceil$  for the low-rank factorization (14) and solve (15) by L-BFGS using *minFunc* [54]. As discussed in Section 3.4, the ACS algorithm is a local optimization algorithm. Fig. 1 shows its performance in the rotation registration experiment with random or RANSAC initialization (experimental setting see Section 5.5). Clearly, with random initialization the proposed algorithm breaks at moderate to high outlier ratios, which implies it may get stuck at poor local minima when without proper initialization.

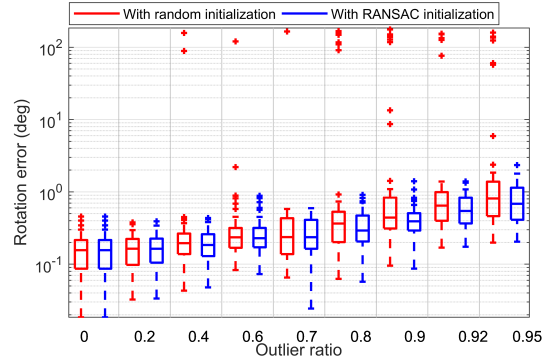


Fig. 1. Rotation error of the proposed algorithm with random or RANSAC initialization in the rotation registration experiment in Section 5.5 (with  $N = 100$  and  $\sigma = 0.01$ ).

#### A. Robust Linear Regression

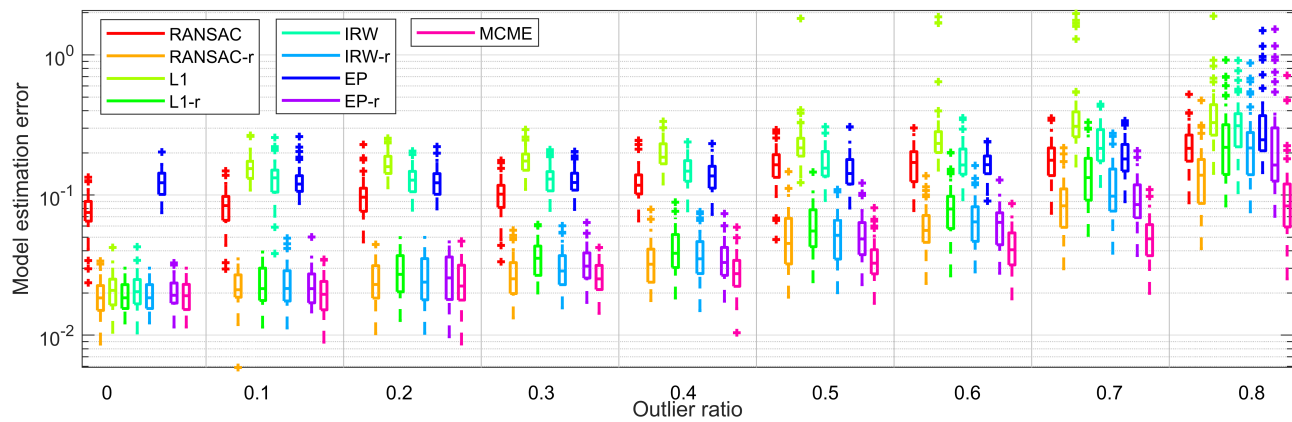
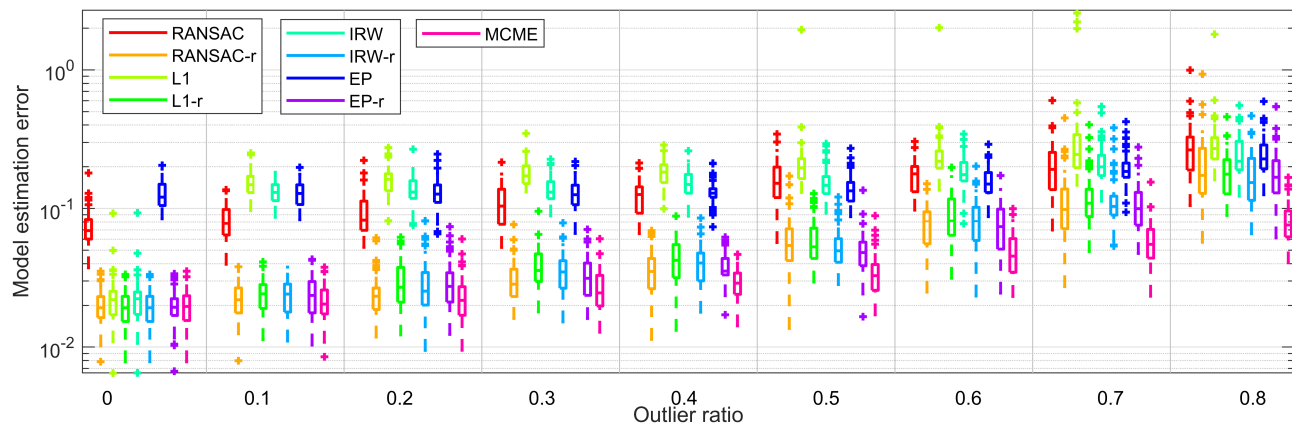
The first experiment considers the robust linear regression problem using synthetic data. The compared algorithms include RANSAC and three deterministic algorithms, the exact penalty method (EP) [21], the L1 method [17], and the iteratively reweighted (IRW) method [18]. A confidence  $\rho = 0.99$  is used in the stopping criterion of RANSAC. For the EP algorithm, we use default parameters of it and employ Gurobi to solve the LP subproblems. Moreover, both EP and MCME are initialized by the solution of the L1 method, and their runtime results include the runtime of the initialization. We generate  $N$  data points  $\{\mathbf{a}_i, b_i\}_{i=1, \dots, N}$  as

$$b_i = \mathbf{a}_i^T \boldsymbol{\theta} + n_i + o_i,$$

where  $\mathbf{a}_i, \boldsymbol{\theta} \in \mathbb{R}^8$ ,  $n_i$  is Gaussian noise with standard deviation of 0.1.  $o_i$  is zero if the data pair  $(\mathbf{a}_i, b_i)$  is inlier, or  $o_i$  is large perturbation if  $(\mathbf{a}_i, b_i)$  is outlier. A randomly selected subset of  $\{b_i\}_{i=1, \dots, N}$  is corrupted by such high noise to simulate outliers. The elements of  $\mathbf{a}_i$  are randomly distributed in  $[-1, 1]$ .

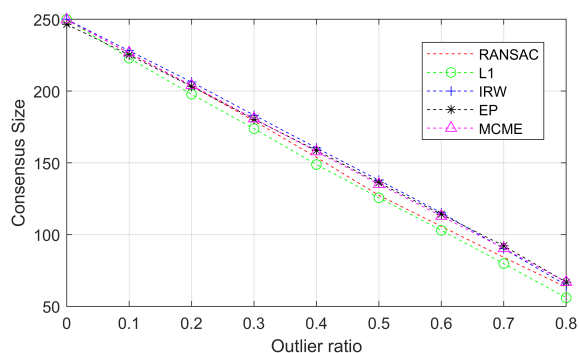
For this model, MCME alternately solves the two subproblems (13) and (12) by the ACS algorithm with the  $\ell_2$  loss (17). The inlier threshold  $\tau$  for the RANSAC, EP, L1 and IRW methods is chosen to bound the inlier residual with a probability of 99.9%, i.e.,  $\mathbb{P}\left((b_i - \mathbf{a}_i^T \boldsymbol{\theta})^2 \leq \tau^2\right) = 1 - 10^{-3}$  for inliers. Under Gaussian noise, it can be computed from the 1-DoF Chi-squared distribution. For MCME, we choose  $\beta = \Phi(\tau) = \tau^2$  according to Proposition 1 and 2. Hence, the inlier thresholds for all the compared algorithms are the same. Since the estimation of  $\boldsymbol{\theta}$  by an MC algorithm is only a feasible solution under inlier residual constraint, we compute a refined LS estimation for each MC algorithm based on its output inliers. This refinement is consistent with the LS fitting of MCME (with  $\Phi$  be the LS loss), which makes the comparison fair. The refinement variants are referred to as RANSAC-r, EP-r, L1-r, and IRW-r.

Fig. 2 shows the estimation error of the algorithms versus outlier ratio for  $N = 250$  in two outlier conditions, uniformly distributed in  $[-2, 2]$  or Gaussian distributed with standard deviation of 2. Given an estimation  $\hat{\boldsymbol{\theta}}$ , the estimation error is defined as  $\|\hat{\boldsymbol{\theta}} - \boldsymbol{\theta}\| / \|\boldsymbol{\theta}\|$ . Each result is an average of

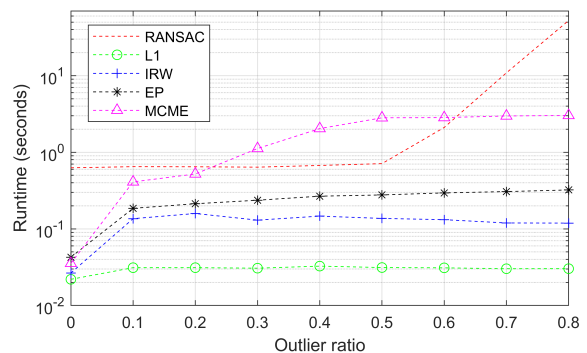
(a) Uniformly distributed outliers in  $[-2, 2]$ 

(b) Gaussian distributed outliers with standard deviation of 2 (which is 20 times that of the inlier noise)

Fig. 2. Model estimation error versus outlier ratio in the linear regression experiment with  $N = 250$ . (a) Uniformly distributed outliers in  $[-2, 2]$ . (b) Gaussian distributed outliers with standard deviation of 2.



(a) Consensus size



(b) Runtime

Fig. 3. Consensus size and runtime comparison in the linear regression experiment with uniformly distributed outliers in  $[-2, 2]$ . (a) Consensus size. (b) Runtime.

50 independent runs. It can be seen that the second-step refinement of each MC method yields much more accurate estimation than the original feasible solution. MCME distinctly outperforms the compared algorithms when the outlier ratio exceeds 20%. Its superiority gets more prominent as the outlier ratio increases, and shows significantly better accuracy than the others at moderate to high outlier ratios. This advantage comes from that MCME takes the fitting residual into consideration in identifying the inliers, while the MC methods do

not.

Fig. 3 compares the consensus size and runtime in the case of uniformly distributed outliers. EP and MCME have similar consensus size. As shown in Proposition 3, the consensus size of an optimum MCME solution is theoretically upper bounded by that of an optimum MC solution. In terms of runtime, the L1 method is the fastest, while MCME is much slower than the L1, EP and IRW methods. As expected, the runtime of RANSAC increases dramatically at high outlier ratios.

TABLE I  
AVERAGE SCORE OF HOMOGRAPHY ESTIMATION ON 20 IMAGE PAIRS  
WITH ALGEBRAIC DISTANCE.

RANSAC/ RANSAC-r	L1/L1-r	IRW/IRW-r	EP/EP-r	MCME
527/6183	12/5870	11/5797	64/6130	6416

### B. Homography Estimation with Algebraic Distance

The second experiment considers homography estimation under algebraic residual model. The homography constraints are linearized as [37, Chapter 4]. We use 20 pairs of images from the VGG dataset (Aerial views I, Corridor, Kapel, Merton II, Merton III, Valbonne Church, Boat, Bark, Bikes, Graff, Trees) and Zurich Building dataset (Building 4, 5, 22, 24, 28, 37, 59, 67, 199). The VLFeat toolbox [48] is employed to extract SIFT features and correspondence matching for each image pair. For the MC algorithms, the inlier threshold is set to  $\tau = 0.5$ , and accordingly for MCME we set  $\beta = \Phi(\tau) = \tau^2$ . Both EP and MCME are initialized by the L1 method.

Since the ground-truth transformation is unknown, we resort to compute a score for the estimated homography based on the symmetric transfer errors [37]. Specifically, with correspondences  $\{(\mathbf{x}_i, \mathbf{x}'_i) : i = 1, 2, \dots, N\}$  and a homography  $\mathbf{H}$ , the score is computed as

$$S(\mathbf{H}) = \sum_i \rho(d^2(\mathbf{x}_i, \mathbf{H}\mathbf{x}'_i)) + \rho(d^2(\mathbf{x}'_i, \mathbf{H}^{-1}\mathbf{x}_i)), \quad (36)$$

where  $d^2$  is the transfer error and

$$\rho(d^2) = \begin{cases} T - d^2, & \text{if } d^2 < T \\ 0, & \text{if } d^2 \geq T \end{cases},$$

with  $T$  being the outlier rejection threshold based on the 2-DoF  $\chi^2$  test at probability of 99% under the assumption that the measurement noise has a standard deviation of 1 pixel. A higher score implies a better estimation of the model, which is usually used to evaluate the quality of an estimated model in practice [49].

Fig. 4 shows the results of the algorithms on the 20 image pairs, including the score computed as (36), consensus size, and runtime. Table 1 shows the average score of estimated homography on the 20 image pairs. Again, it can be observed that, for the four MC algorithms, the second-step refinement helps to attain significant better estimation. MCME achieves the highest average score. Fig. 5(a) presents some sample qualitative results of MCME.

### C. Homography Estimation with Geometric Distance

The third experiment considers homography estimation under geometric residual model. For the MC methods, the residual constraint (19) with  $\ell_1$ -norm is used with a linearization. For MCME, the loss (20) is used. It has been shown in [39] that the  $\ell_2$  and  $\ell_\infty$  methods generally have very similar performance in homography estimation with geometric distance. The inlier threshold is set to  $\tau = 4$  pixels for the MC methods, while  $\beta = \tau^2$  is used for MCME. EP and MCME are initialized by RANSAC, as it can yield better performance than L1 initialization in this experiment. We use the same data in the second experiment.

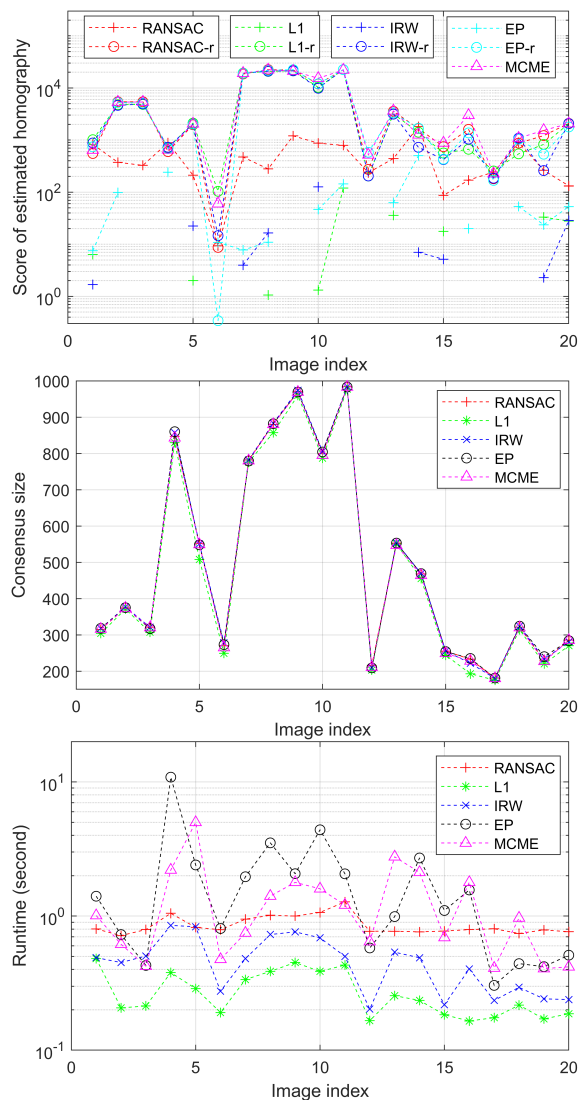


Fig. 4. Homography estimation results on 20 image pairs with algebraic distance. From top to bottom are respectively the score of estimated homography, consensus size, and runtime.

TABLE II  
AVERAGE SCORE OF HOMOGRAPHY ESTIMATION ON 20 IMAGE PAIRS  
WITH GEOMETRIC DISTANCE.

RANSAC/ RANSAC-r	L1/L1-r	IRW/IRW-r	EP/EP-r	MCME
8135/8706	5709/7656	7202/8050	7644/8515	8773

Fig. 6 presents the results of the algorithms on the 20 image pairs, including the score computed as (36), consensus size, and runtime. Table 2 shows the average score of estimated homography over the 20 image pairs. It can be seen that under geometric distance, the second-step refinement of the MC methods also helps to attain distinctly better accuracy. Noteworthily, MCME achieves the highest score on 12 image pairs, while gives the largest consensus size on 18 image pairs. It is worth noting that, from Proposition 3, the consensus size of an optimum MCME solution is upper bounded by that of an optimum MC solution. However, as both the problems are nonconvex binary optimization problems, none of the com-

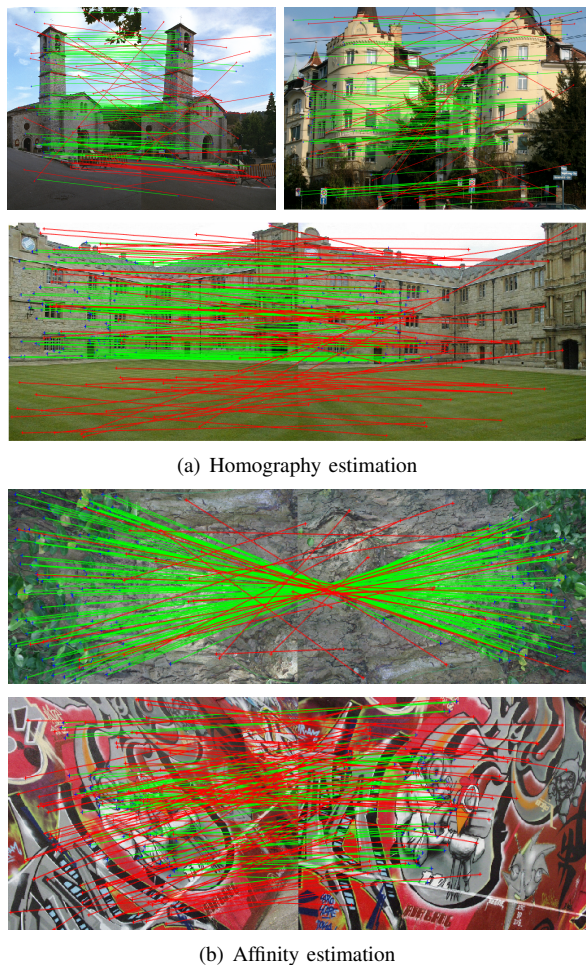


Fig. 5. Sample qualitative results of MCME in (a) homography estimation, and (b) affinity estimation. Red and green lines represent identified inliers and outliers, respectively (only 100 inliers/outliers are displayed for clarity).

pared algorithms is guaranteed to find an optimum solution. Hence, the larger consensus size of MCME demonstrates that the proposed algorithm is more effective in handling the underlying intractable binary optimization problem. From Table 1 and 2, for all the compared methods, geometric distance yields significantly higher scores than algebraic distance. Moreover, MCME achieves the highest average score.

#### D. Affinity Estimation

As introduced in Section 4.1, for affine transformation, the geometric and algebraic distances are identical. We use the Boat, Bark, Bikes, Graff, and Trees images from the Oxford VGG’s affine image dataset. Two images pairs are picked out from each scene, which results in 10 image pairs for test. Similarly, SIFT features and correspondence matching are extracted by the VLFeat toolbox. We set an inlier threshold of  $\tau = 1$  pixel for the MC algorithms, while  $\beta = \Phi(\tau) = \tau^2$  for MCME. As the ground-truth transformation is unknown, we also compute a score for an estimation based on the symmetric transfer errors. For an affinity  $\Theta \in \mathbb{R}^{2 \times 3}$  satisfying  $\mathbf{x}_i = \Theta \tilde{\mathbf{x}}'_i$ , the score is computed for  $\mathbf{H} = \begin{bmatrix} \Theta \\ 0 & 0 & 1 \end{bmatrix}$  by (36).

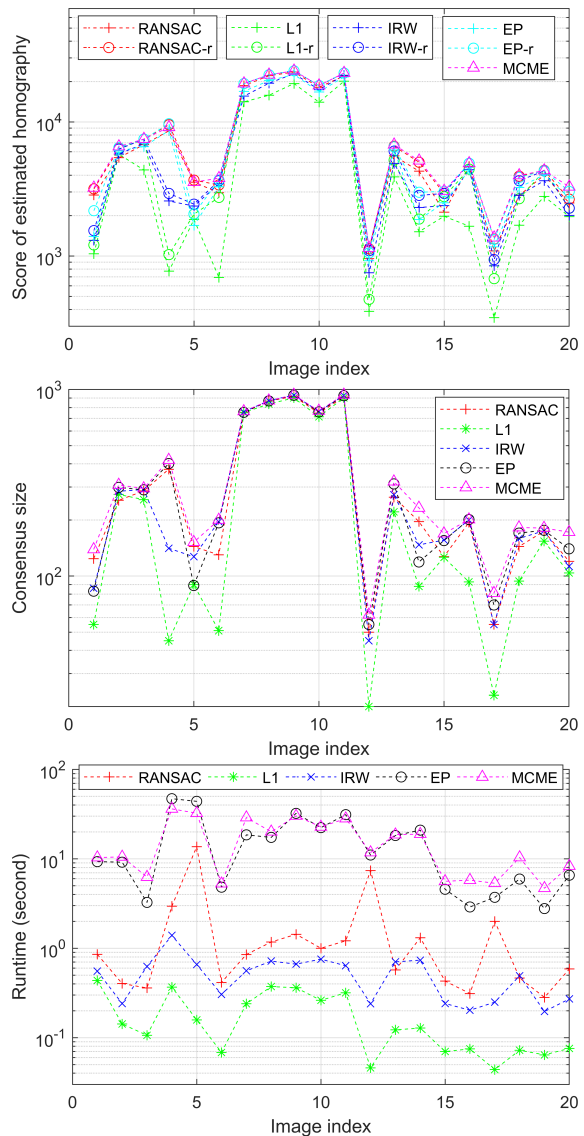


Fig. 6. Homography estimation results on 20 image pairs with geometric distance. From top to bottom are respectively the score of estimated homography, consensus size, and runtime.

TABLE III  
AVERAGE SCORE OF AFFINITY ESTIMATION ON 10 IMAGE PAIRS.

RANSAC/ RANSAC-r	L1/L1-r	IRW/IRW-r	EP/EP-r	MCME
9601/9688	9297/9498	9634/9697	9709/9715	9784

Table 3 compares the average score of the methods, whilst Fig. 5(b) shows sample qualitative results of MCME. Again, MCME achieves the highest average score. In the affinity estimation, the performance gap between the methods is not so prominent as that in the homography estimation experiment.

#### E. Rotation Registration

The fifth experiment evaluates MCME on rotation search, in comparison with *i)* RANSAC; *ii)* GORE-RANSAC, which uses GORE [50] to firstly remove most outliers and then uses RANSAC to estimate the model based on the pruned measure-

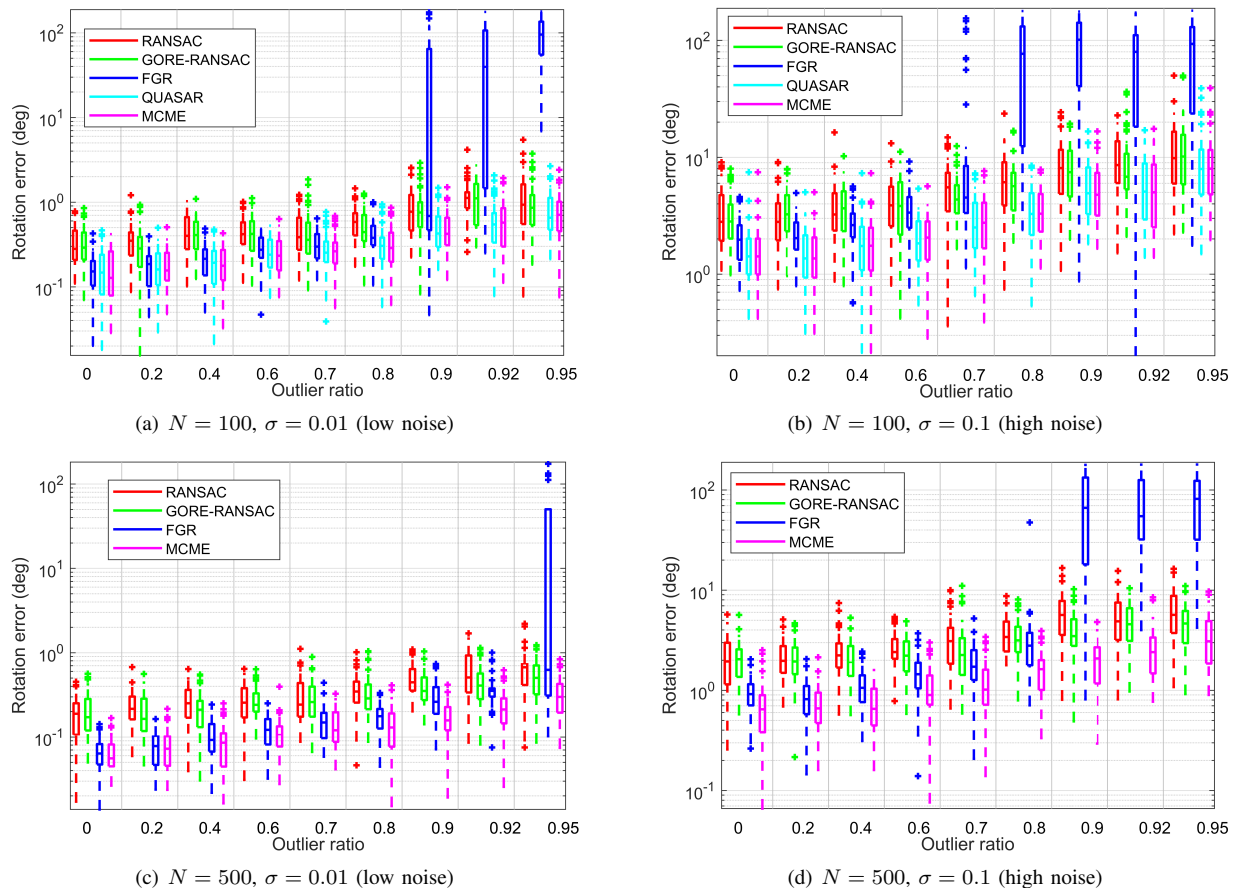


Fig. 7. Rotation error comparison in the rotation registration experiment with low and high noise conditions. (a)  $N = 100, \sigma = 0.01$ . (b)  $N = 100, \sigma = 0.1$ . (c)  $N = 500, \sigma = 0.01$ . (d)  $N = 500, \sigma = 0.1$ . QUASAR is not compared in the case of  $N = 500$  as it runs out of memory when  $N > 150$ .

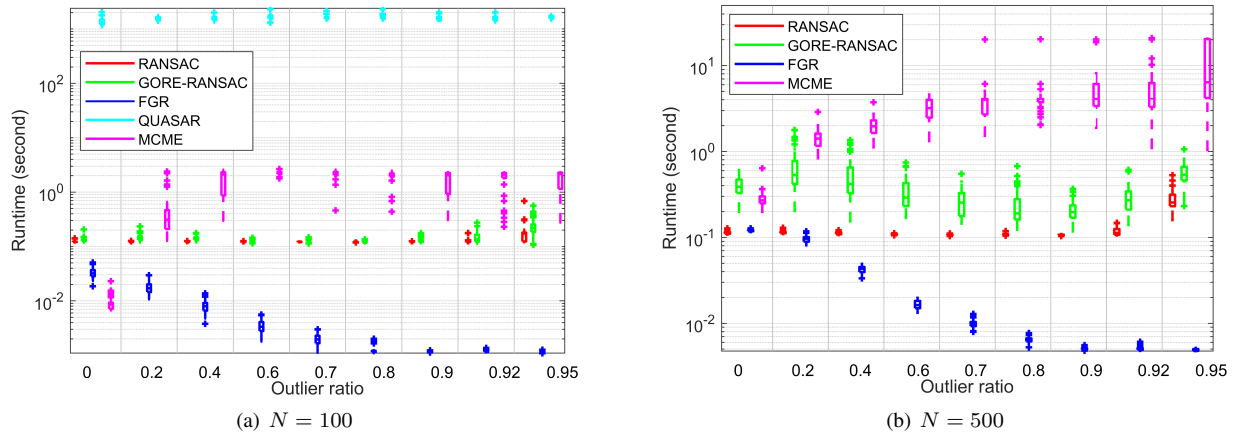


Fig. 8. Runtime comparison in the rotation registration experiment for two cases, (a)  $N = 100$ , and (b)  $N = 500$  (with  $\sigma = 0.1$ ).

ments; *iii*) Fast global registration (FGR) [30]; *iv*) QUASAR [31], which is implemented in Matlab using CVX [32] with MOSEK [52] as the SDP solver. Note that GORE can achieve guaranteed outlier removal and can provide a rough estimation of the model from the pruned data, but GORE-RANSAC has significantly better accuracy in most cases. For QUASAR and MCME, we use the same noise bound parameter  $\beta = \bar{c}^2 \sigma^2$  such that  $\mathbb{P}(\|\mathbf{b}_i - \mathbf{R}\mathbf{a}_i\|^2 \leq \bar{c}^2 \sigma^2) = 1 - 10^{-6}$  holds for inliers, which under Gaussian inlier noise can be computed

from the 3-DoF Chi-squared distribution. For the rotation registration problem, MCME alternately solves the two subproblems (13) and (25). We use the RANSAC solution as the initialization of MCME. All the runtime results of MCME include the runtime of the RANSAC initialization.

The Bunny dataset from the Stanford 3D Scanning Repository [53] is used. Firstly, the point cloud is resized into a unit cube  $[0, 1]^3$  and randomly down-sampled to  $N$  points with  $N \in \{100, 500\}$ . Then, a random rotation is applied and

additive noise and outliers are randomly generated according to (22). Two conditions with low and high inlier noise are considered, with  $\sigma = 0.01$  and  $\sigma = 0.1$ , respectively. Meanwhile, different outlier ratios from 0 to 95% are considered. Each result is an average of 50 independent runs.

Fig. 7 presents the rotation error of the algorithms in the two noise conditions for  $N = 100$  and  $N = 500$ , respectively. It can be seen that FGR performs well at low outlier ratios, but tends to beak at relatively high outlier ratios, e.g., when the outlier ratio exceeds 70% in the case of  $N = 100$  and  $\sigma = 0.1$ . GORE-RANSAC generally has better performance than RANSAC as it firstly removes most of the outliers by the GORE method. For  $N = 100$ , QUASAR and MCME generally performs comparably and outperform the others. In the case of  $N = 500$ , QUASAR is not compared as it runs out of memory when  $N > 150$ . For  $N = 500$ , MCME distinctly outperforms its counterparts in most cases, and the advantage is especially conspicuous in the high noise case.

Fig. 8 compares the runtime of the algorithms. Clearly, FGR is the fastest. Though both QUASAR and MCME involve solving SDP, MCME is more than 3 orders of magnitude faster than QUASAR in the case of  $N = 100$ . This thanks to the accelerating strategy using low-rank factorization and the unconstrained formulation exploiting the sparsity of the problem. However, QUASAR cannot be accelerated like MCME as it has a large number of constraints as explained in Remark 4. Although the computational complexity of MCME increases more rapidly than FGR, RANSAC and GORE-RANSAC as  $N$  increases, MCME can scale to relatively large problem size.

#### F. 6-DoF Euclidean Registration

The final experiment evaluates MCME in 6-DoF rigid registration, where both rotation and translation need to be estimated. We generate the data measurements similar to the rotation registration experiment except that a random translation is additionally considered according to (33). In this setting, MCME alternately solves the two subproblems (13) and (35). The TEASER++ algorithm (implemented in C++) [51] is also compared in this experiment. TEASER++ decouples the scale, rotation and translation estimation and solves them separately and sequentially. It solves decoupled scale and translation estimation via adaptive voting, and solves the rotation estimation via a graduated nonconvexity scheme [29], which has shown highly effectiveness and efficiency. The noise bound parameter of TEASER++ is tuned to provide the best performance.

Fig. 9 presents the rotation error, translation error and runtime of the compared algorithms for  $N = 200$ . Similar to the rotation registration experiment, two noise conditions with  $\sigma = 0.01$  and  $\sigma = 0.1$  are considered. It can be seen that FGR tends to break at high outlier ratios, especially in the high noise condition, e.g. when the outlier ratio exceeds 50%. MCME achieves the best accuracy in most cases, and its advantage gets more prominent in the high noise condition. It again significantly outperforms the RANSAC and GORE-RANSAC methods. Moreover, the results demonstrate the highly efficiency of FGR and TEASER++, which are much

faster than MCME. Fig. 10 illustrates a typical registration example by RANSAC and MCME at an outlier ratio of 80%.

## VI. CONCLUSION

A new formulation, namely MCME, has been proposed to achieve simultaneous consensus maximization and model fitting. It takes fitting residual into account in finding inliers, and is theoretically shown to have lower fitting residual than traditional maximum consensus robust fitting. An alternating minimization algorithm with embedded semidefinite relaxation is developed, which is further accelerated by utilizing low-rank factorization and exploiting the sparsity of the problem. Experimental results demonstrated that MCME can achieve better accuracy than RANSAC and deterministic approximate maximum consensus methods at high outlier ratios. It also compares favorably with state-of-the-art registration methods in rotation and Euclidean registration, especially in the presence of high noise and outliers.

## REFERENCES

- [1] T. J. Chin and D. Suter, "The maximum consensus problem: recent algorithmic advances," *Synthesis Lectures on Computer Vision* (Eds. Gerard Medioni and Sven Dickinson), Morgan and Claypool Publishers, San Rafael, CA, USA, Feb 2017.
- [2] P. Meer, "Robust techniques for computer vision," in G. Medioni and S. B. Kang eds.: *Emerging topics in computer vision*. Prentice Hall, pp. 107–190, 2004.
- [3] D. Martinec and T. Pajdla, "Robust rotation and translation estimation in multiview reconstruction," in *IEEE Conf. Computer Vision and Pattern Recognition (CVPR)*, 2007.
- [4] M. Brown and D. G. Lowe, "Automatic panoramic image stitching using invariant features," *Int. J. Computer Vision*, vol. 74, no. 1, pp. 59–73, 2007.
- [5] M. A. Fischler and R. C. Bolles, "Random sample consensus: a paradigm for model fitting with applications to image analysis and automated cartography," *Communications of the ACM*, vol. 24, no. 6, pp. 381–395, 1981.
- [6] O. Chum, J. Matas, and J. Kittler, "Locally optimized ransac," in *DAGM*, Springer, 2003.
- [7] B. J. Tordoff and D. W. Murray, "Guided-mlesac: Faster image transform estimation by using matching priors," *IEEE Trans. Pattern Analysis and Machine Intelligence*, vol. 27, no. 10, pp. 1523–1535, 2005.
- [8] O. Chum and J. Matas, "Matching with PROSAC–Progressive sample consensus," in *IEEE Conf. Computer Vision and Pattern Recognition (CVPR)*, Jun. 2005, pp. 220–226.
- [9] S. Choi, T. Kim, and W. Yu, "Performance evaluation of RANSAC family," in *British Machine Vision Conference (BMVC)*, 2009.
- [10] K. Lebeda, J. Matas, and O. Chum, "Fixing the locally optimized ransac–Cfull experimental evaluation," in *British Machine Vision Conference*, 2012, pp. 1–11.
- [11] H. Li, "Consensus set maximization with guaranteed global optimality for robust geometry estimation," in *IEEE Conf. Computer Vision and Pattern Recognition (CVPR)*, 2009, pp. 1074–1080.
- [12] Y. Zheng, S. Sugimoto, and M. Okutomi, "Deterministically maximizing feasible subsystem for robust model fitting with unit norm constraint," in *IEEE Conf. Computer Vision and Pattern Recognition (CVPR)*, 2011, pp. 1825–1832.
- [13] P. Speciale, D. P. Paudel, M. R. Oswald, T. Kroeger, L. V. Gool, and M. Pollefeys, "Consensus maximization with linear matrix inequality constraints," in *IEEE Conf. on Computer Vision and Pattern Recognition (CVPR)*, July 2017, pp. 5048–5056.
- [14] T. J. Chin, P. Purkait, A. Eriksson, and D. Suter, "Efficient globally optimal consensus maximisation with tree search," in *IEEE Conf. Computer Vision and Pattern Recognition (CVPR)*, 2015, pp. 2413–2421.
- [15] O. Enqvist, E. Ask, F. Kahl, and K. Astrom, "Robust fitting for multiple view geometry," in *European Conference on Computer Vision*, 2012, pp. 738–751.
- [16] C. Olsson, O. Enqvist, and F. Kahl, "A polynomial-time bound for matching and registration with outliers," in *IEEE Conf. Computer Vision and Pattern Recognition (CVPR)*, 2008, pp. 1–8.

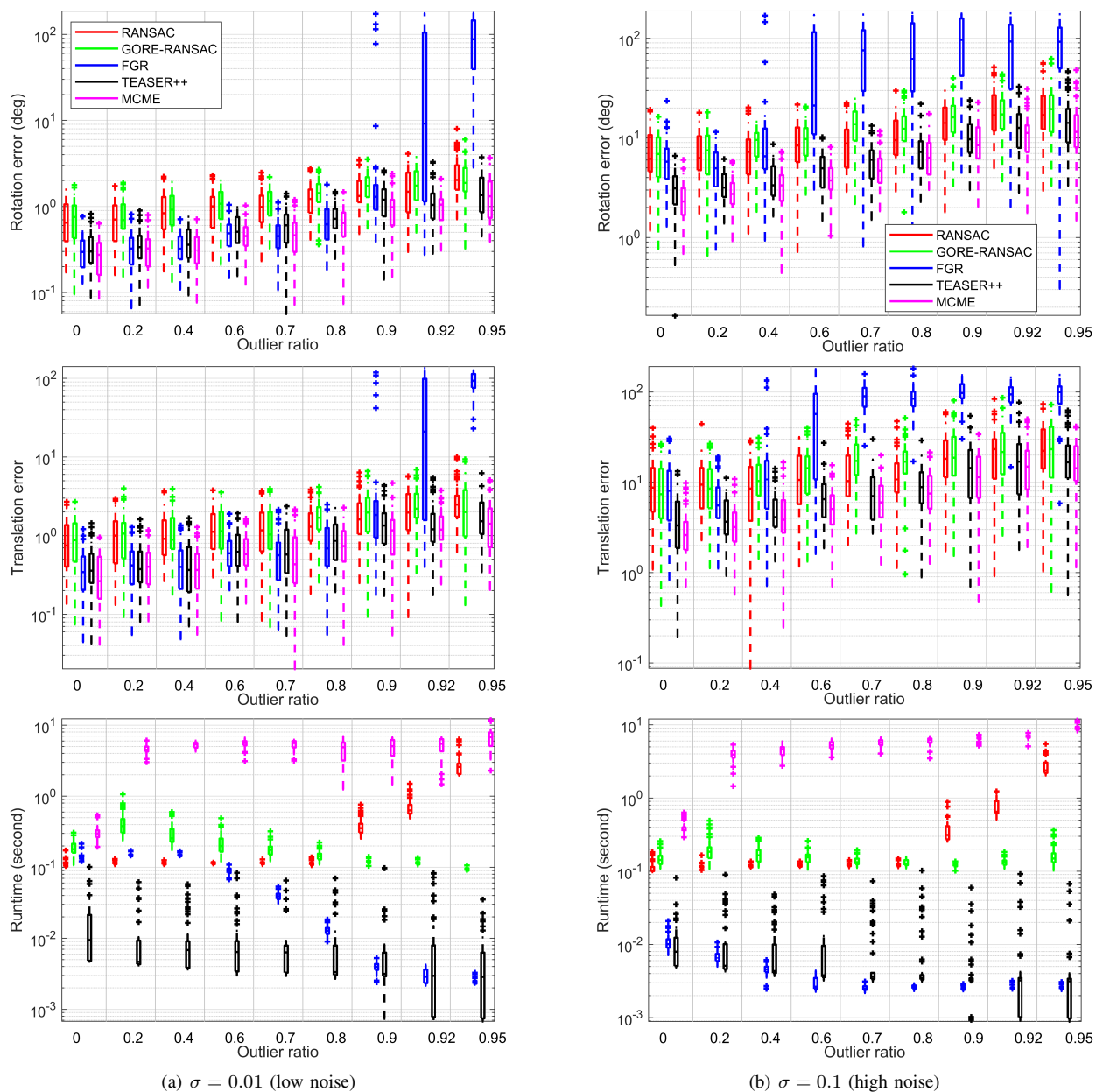


Fig. 9. Rotation error, translation error and runtime comparison in the 6-DoF Euclidean registration experiment. (a)  $\sigma = 0.01$ . (b)  $\sigma = 0.1$ .

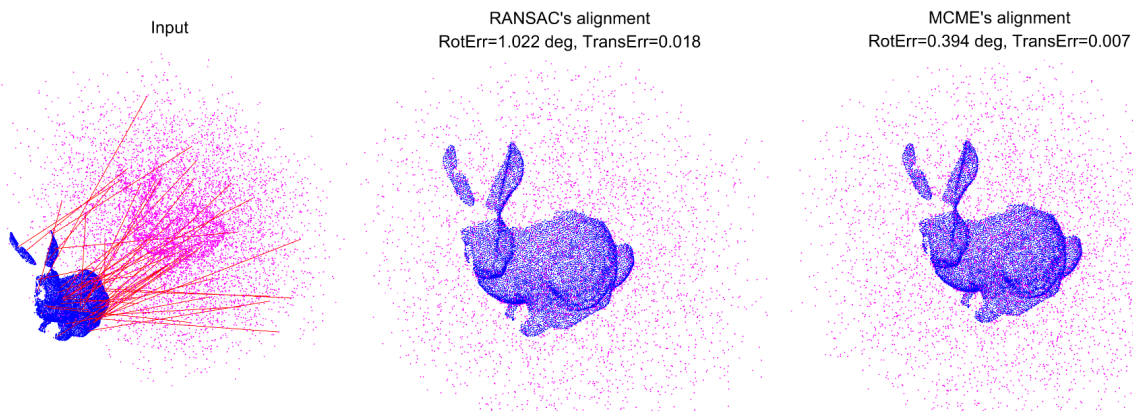


Fig. 10. Illustration of 6-DoF Euclidean registration by RANSAC and MCME (with outlier ratio being 80%), along with the rotation error (RotErr) and translation error (TransErr).

- [17] C. Olsson, A. P. Eriksson, and R. Hartley, "Outlier removal using duality," in *IEEE Conf. Computer Vision and Pattern Recognition (CVPR)*, pp. 1450–1457, 2010.
- [18] P. Purkait, C. Zach, and A. Eriksson, "Maximum consensus parameter estimation by reweighted L1 methods," in *Int. Workshop on Energy Minimization Methods in Computer Vision and Pattern Recognition*, 2018, pp. 312–32.
- [19] F. Wen, R. Ying, Z. Gong, and P. Liu, "Efficient algorithms for maximum consensus robust fitting," *IEEE Trans. Robotics*, vol. 36, no. 1, pp. 92–106, Feb. 2020.
- [20] H. Le, T. J. Chin, and D. Suter, "An exact penalty method for locally convergent maximum consensus," in *IEEE Conf. Computer Vision and Pattern Recognition (CVPR)*, 2017, pp. 1888–1896.
- [21] H. Le, T. J. Chin, A. Eriksson, and D. Suter, "Deterministic approximate methods for maximum consensus robust fitting," *IEEE Trans. Pattern Analysis and Machine Intelligence*, 2019.
- [22] K. Sim and R. Hartley, "Removing outliers using the 1-infinity norm," in *IEEE Conf. Computer Vision and Pattern Recognition (CVPR)*, 2006, pp. 485–494.
- [23] Y. Seo, H. Lee, and S. W. Lee, "Outlier removal by convex optimization for 1-infinity approaches," in *Pacific Rim Symposium on Advances in Image and Video Technology (PSIVT)*, 2009.
- [24] S. Poljak, F. Rendl, and H. Wolkowicz, "A recipe for semidefinite relaxation for (0, 1)-quadratic programming," *Journal of Global Optimization*, vol. 7, no. 1, pp. 51–73, 1995.
- [25] S. Burer and R. D. C. Monteiro, "A nonlinear programming algorithm for solving semidefinite programs via low-rank factorization," *Mathematical Programming*, vol. 95, no. 2, pp. 329–357, 2003.
- [26] Z. Zhang, "Determining the epipolar geometry and its uncertainty: A review," *Int. J. of Computer Vision*, vol. 27, no. 2, pp. 161–195, 1998.
- [27] P. H. S. Torr and A. Zisserman, "MLESAC: A new robust estimator with application to estimating image geometry," *Comput. Vis. Image Understand.*, vol. 78, no. 1, pp. 138–156, 2000.
- [28] K. Aftab and R. Hartley, "Convergence of iteratively re-weighted least squares to robust m-estimators," in *IEEE Winter Conf. on Applications of Computer Vision*, 2015, pp. 480–487.
- [29] H. Yang, P. Antonante, V. Tzoumas, and L. Carlone, "Graduated nonconvexity for robust spatial perception: From non-minimal solvers to global outlier rejection," *IEEE Robotics and Automation Letters*, 2020.
- [30] Q. Y. Zhou, J. Park, and V. Koltun, "Fast global registration," in *European Conf. on Computer Vision (ECCV)*, pp. 766–782, 2016.
- [31] H. Yang and L. Carlone, "A quaternion-based certifiably optimal solution to the Wahba problem with outliers," in *IEEE Int. Conf. Computer Vision (ICCV)*, 2019.
- [32] M. Grant, S. Boyd, and Y. Ye. *CVX: Matlab software for disciplined convex programming*, 2014.
- [33] G. Pataki, "On the rank of extreme matrices in semidefinite programs and the multiplicity of optimal eigenvalues," *Mathematics of Operations Research*, vol. 23, pp. 339–358, 1998.
- [34] N. Boumal, V. Voroninski, and A. Bandeira, "The non-convex Burer-Monteiro approach works on smooth semidefinite programs," in *Advances in Neural Information Processing Systems*, 2016, pp. 2757–2765.
- [35] S. Homer and M. Peinado, "Design and performance of parallel and distributed approximation algorithm for the maxcut," *J. of Parallel and Distributed Computing*, vol. 46, pp. 48–61, 1997.
- [36] R. Fletcher. *Practical Methods of Optimization*. John Wiley and Sons, New York, second edition, 1987.
- [37] R. Hartley and A. Zisserman. *Multiple View Geometry in Computer Vision*. Cambridge university press, 2003.
- [38] Q. Ke and T. Kanade, "Quasiconvex optimization for robust geometric reconstruction," *IEEE Trans. Pattern Analysis and Machine Intelligence*, vol. 29, no. 10, pp. 1834–1847, 2007.
- [39] F. Kahl and R. Hartley, "Multiple view geometry under the  $\ell_\infty$ -norm," *IEEE Trans. Pattern Analysis and Machine Intelligence*, vol. 30, no. 9, pp. 1603–1617, 2008.
- [40] Y. Seo and R. Hartley, "A fast method to minimize  $\ell_\infty$  error norm for geometric vision problems," in *IEEE Conf. Computer Vision and Pattern Recognition (CVPR)*, 2007.
- [41] J. Gorski, F. Pfeuffer, and K. Klamroth, "Biconvex sets and optimization with biconvex functions: a survey and extensions," *Mathematical Methods of Operations Research*, vol. 66, no. 3, pp. 373–407, 2007.
- [42] G. Wahba, "A least squares estimate of satellite attitude," *SIAM review*, vol. 7, no. 3, pp. 409–409, 1965.
- [43] J.-C. Bazin, Y. Seo, R. Hartley, and M. Pollefeys, "Globally optimal inlier set maximization with unknown rotation and focal length," in *European Conf. on Computer Vision (ECCV)*, pp. 803–817, 2014.
- [44] R. I. Hartley and F. Kahl, "Global optimization through rotation space search," *Int. J. of Computer Vision*, vol. 82, no. 1, pp. 64–79, 2009.
- [45] J. P. Iglesias, C. Olsson, and F. Kahl, "Global optimality for point set registration using semidefinite programming," in *IEEE Conf. on Computer Vision and Pattern Recognition (CVPR)*, 2020.
- [46] J.-C. Bazin, Y. Seo, and M. Pollefeys, "Globally optimal consensus set maximization through rotation search," in *Asian Conference on Computer Vision*, 2012, pp. 539–551.
- [47] M. D. Shuster, "A survey of attitude representations," *Journal of the Astronautical Sciences*, vol. 41, no. 4, pp. 439–517, 1993.
- [48] A. Vedaldi and B. Fulkerson, "Vlfeat: An open and portable library of computer vision algorithms," in *ACM Int. Conf. on Multimedia*, 2010, pp. 1469–1472.
- [49] R. Mur-Artal, J. M. M. Montiel, and J. D. Tardos, "Orb-slam: a versatile and accurate monocular slam system," *IEEE Trans. on Robotics*, vol. 31, no. 5, pp. 1147–1163, 2015.
- [50] A. P. Bustos and T. J. Chin, "Guaranteed outlier removal for point cloud registration with correspondences," *IEEE Trans. Pattern Analysis and Machine Intelligence*, vol. 40, no. 12, pp. 2868–2882, 2017.
- [51] H. Yang, J. Shi, and L. Carlone, "Teaser: Fast and certifiably point cloud registration," *Preprint, arXiv:2001.07715*, 2020.
- [52] MOSEK ApS. *The MOSEK optimization toolbox for MATLAB manual*. Version 8.1., 2017.
- [53] B. Curless and M. Levoy, "A volumetric method for building complex models from range images," in *SIGGRAPH*, pp. 303–312, 1996.
- [54] M. Schmidt. *minFunc: unconstrained differentiable multivariate optimization in Matlab*. 2005.